UNIVERSITY OF OKLAHOMA

GRADUATE COLLEGE

COMPARISON OF DISCRETE PART VERIFICATION USING COORDINATE
MEASURING MACHINE AND ARTICULATED ARM COORDINATE MEASURING
MACHINE

A THESIS

SUBMITTED TO THE GRADUATE FACULTY

in partial fulfillment of the requirements for the

Degree of

MASTER OF SCIENCE

By

ANDREA LOPEZ PULGARIN

Norman, Oklahoma

2019

COMPARISON OF DISCRETE PART VERIFICATION USING COORDINATE
MEASURING MACHINE AND ARTICULATED ARM COORDINATE MEASURING
MACHINE

A THESIS APPROVED FOR THE
SCHOOL OF INDUSTRIAL AND SYSTEMS ENGINEERING

BY THE COMMITTEE CONSISTING OF

Dr. Shivakumar Raman, Chair

Dr. Janet K. Allen

Dr. Theodore Trafalis

To God… because we keep making him laugh with our plans!

To my husband, Felipe. Thanks for being my support.

Acknowledgments

Table of Contents

List of Figures

List of Tables

Abstract

Quality assurance is key in manufacturing and assembling processes and is usually implemented by specifying and controlling tolerances and surface finish of important features, in discrete product manufacturing industry. Much of product verification and inspection for single parts and assemblies are considered to be non-value added, and hence, the processes and procedures must be constantly improved to achieve better savings in time and cost.

Coordinate Measuring Machines (CMMs) are the gold standard for geometry verification of parts in the industry, for their consistency and accuracy. Articulated Arm CMMs (AACMMs) use a scan/arm configuration, and as such are considered not accurate enough in part verification. And yet, they can result in many time-savings and ease of operation. If developed suitably, these can be used quite viably in situations that do not demand high accuracies. It is the aim of this thesis to investigate how the AACMMs compare to the traditional gantry CMMs in flatness verification. Flatness verification is the most fundamental of geometry verification employed in the industry. The success achieved in form verification can be extended to investigate further geometries, and AACMMs can be developed as an economical alternative to the more traditional CMMs in industry.

Specifically, this thesis investigated the flatness of surfaces generated by milling (roughing and finishing). Experiments were conducted on three rectangular blocks of Steel 1018 and three more of Aluminum 6061 of specific dimensions. The CMM employed was used to collect data using three sampling strategies: Hammersley, Halton Zaremba, and Aligned systematic methods. The AACMM was also used to collect the flatness data on each plate through a scan. A commercial Geomagic® Control X™ was used to find flatness deviation between measured data and the CAD model for each of the rough and finish surfaces. Statistics from the distribution of gap distance and deviations were presented through the study. The accuracy was noted in each case.

The results developed verified that AACMM is not as accurate as of the traditional CMM in measuring flatness. All the same, the results were sufficient to suggest that AACMM can be used as a viable and faster alternative to the CMM in flatness verification.

CHAPTER 1: Introduction

1. Summary

Metrology, or the science of measurement, is critical in achieving high standards of quality control of parts in the manufacturing industry. It often verifies that the different geometries of the part are made according to the design specifications. Design, manufacturing and final product all are linked accomplishing a functional part that will be accepted. The verification process of parts in the industry is not considered to add value, rather it is a post-process operation that consumes resources of time and money. Metrology has tried to solve this problem using different technologies and systematic processing of the information to improve the results. Although it has been successful in verifying complex geometries, there is much room for improvement and incorporation of new methodologies.

Some important definitions required to understand metrology better are:

- geometric features which provide a description of either a physical section or design of a part, and

- geometric tolerances or the allowable variations for a part dimension in size, form, orientation, or location.

Literature in metrology keeps adapting to new technologies and methodologies. The objective is to have more impact on design and process planning. There are several instruments that help in the measurement of geometries, from manual gauges to stylus-type instruments. One of the most used equipments for part verification is the coordinate measuring machine, that allows for the measurement of geometric features by using a stylus that senses the location and provides a coordinate measurement with (X, Y, Z) components. Coordinate metrology evolves from the use of the rigid body Coordinate Measuring Machines (CMMs) that typically give accuracies 0.0002 into Articulated Arm Coordinate Measuring Machines (AACMMs) or flexible body arms that give 0.0014in. The former requires specialized operators and inspectors, uses sampling methods to survey the surface and requires a certain quantity of points that will represent the surface created by manufacturing processes. It also requires implementing fitting algorithms and error calculation methods to find the geometric deviation. This usually results in more time and resources to process all the information. The latter is a low accuracy alternative for measuring geometric features but provides a few advantages. The AACMMs are easier to use and require less specialized operators

to measure with them. Although the AACMM also uses probes, some are also equipped with laser scanners that allow inspecting the geometric features faster. Both systems use software for sampling and fitting and provide the user with programmable flexibility.

Measurement and inspection are usually subject to error. This error comes from different sources. One source of error is equipment error caused due to gravity, degrees of freedom, and kinematics. Another source, human error, can be attributed to the operator who takes the measurements. To put this research in context, we try to explain some important concepts used herein.

1.1 Surface Texture and Roughness

When sampling a part, we are measuring the differences in the surface, to understand roughness, it is necessary to say that surfaces have their own attributes; all this is called surface texture. Among the many features that form surface texture are flaws which are defects such as scratches, cracks, dents or holes. The pattern that can be seen on the surface is called lay. Roughness is considered to be small-scale irregular deviations and is measured in width, height and distance spacing on the surface, on the other hand, waviness is the deviation from the flat surface at a larger scale than roughness, and it is measured in terms of the distance between longer-term crests and the height between valleys and crests. Figure 1 shows the different surface texture components on one of the parts studied.

1.2 Manufacturing Process

Manufacturing deals with the different processes that are required to produce an item. Generally, it starts with a raw material that is subject to a series of processes that make individual contributions in the shaping of the desired part. Each of these processes adds value to the product. (Kalpakjian, Serope - Schmid, 2014). To transform raw material into a product it generally undergoes several manufacturing processes. Among the most common processes are turning, boring, milling and drilling.
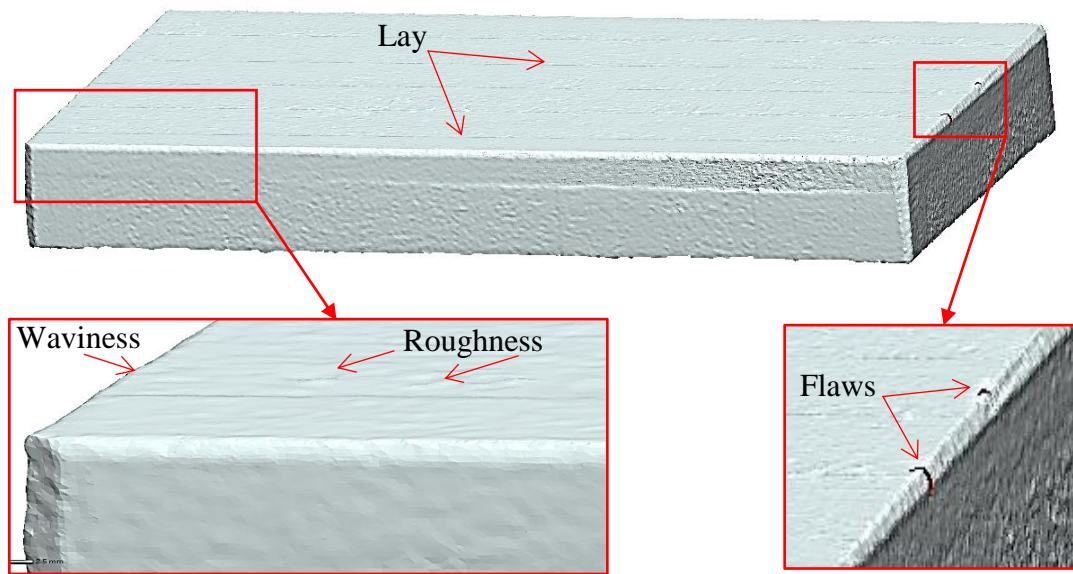
Figure 1. Surface Roughness Concepts

For this thesis, we used face milling, and more specifically multi-pass face milling, to machine the parts that are measured using the two measuring instruments. Both rough and finish milling are employed on the top surface of the parts.

This operation is usually carried out at high feed rates and large depths, and the primary objective is to remove material. Tolerances and finish are usually not as important during a rough pass, as a finish pass would be employed to achieve those. (Kalpakjian, Serope - Schmid, 2014)(Kalpakjian, Serope - Schmid, 2014)(Kalpakjian, Serope - Schmid, 2014)(Kalpakjian, Serope - Schmid, 2014)(Kalpakjian, Serope - Schmid, 2014)(Kalpakjian, Serope - Schmid, 2014)(Kalpakjian, Serope - Schmid, 2014)(Kalpakjian, Serope - Schmid, 2014)Finish passes are made often at high speeds, lower feed rates and smaller depths of cut. They result in smoother and more precise surfaces than rough passes.

1.3 Form Tolerance Verification for Flatness

This research deals with the deviation of flatness from perfect shape and comparison of deviations obtained with two different types of apparatus. First, we will explain flatness and how

it is verified, Flatness is represented by the Feature Control symbol (ANSI Y14.5M, 1982) as shown in *Table 1*.

Type of Tolerance	Characteristic	Symbol
Form	Flatness	▱

Table 1. Flatness Geometric Characteristic and Symbol

Flatness is defined as the elements contained in a plane, and the form tolerance is the minimum separation between two parallel planes that envelop all the form deviations of the surface. (ASME, 2009)**.** There are many sampling and zone fitting strategies that are used to calculate flatness.

Three different sampling methods are studied in this work: aligned systematic, Hammersley and Halton-Zaremba. We will go in-depth about these methods in the literature review and methodology sections to understand why we use them to verify flatness and accuracy based on the number of points taken for the sampling (Kim & Raman, 2000). The discrete points were measured from the top surface of the parts using a CMM obtaining actual coordinate points that denote the surface. The top surface was also surveyed with a scanner using an AACMM, thus obtaining a cloud of points to represent the surface. The measuring capabilities of each machine were studied through experimental data collection and analysis.

1.4 Problem Definition and Objective

With the automation revolution, there has been a great shift not only in new technology but on processes and how to make them more efficient. It is expected that now that parts are manufactured in less time, verification of the specifications will also consume less time, so quality control adds value to the product instead of taking more resources for sophisticated measurement methods.

CMMs are the current industry standard for the measurement and verification of manufactured surfaces. AACMMs, although employed in reverse engineering studies, are often never used in geometry verification. The former is very time consuming but presents better precision and accuracy while the latter is faster and requires less skill in its operation. This research proposes to compare the flatness measurements made by using these machines.

Previous research has focused on the calibration of AACMM as compared to CMM. Important topics range from using the laser tracker as a reference instrument (Acero, Brau, Santolaria, & Pueo, 2015), revision comparison of calibration results, showing why they are more accessible in the price range and used in industry (Gromczak, Ostrowska, Owczarek, & Sładek, 2015). And lastly, measurement uncertainties and its main cause are discussed by (Ge et al., 2014).

In the studies for AACMM, no comparison of measurements between CMM and articulated arms is evident. This is a research gap worth of study to the industry since there is interest in using AACMMs on shop floors for quality verification of manufactured parts.

1.5 Contributions

This thesis will research different sampling methods to better describe flatness measurement by CMMs. It will also create a pilot study to investigate the differences in measurement results obtained using CMM and AACMM. Data processing and analysis is expected to provide better guidance to designers, manufacturers, and part inspectors. It is also expected that systematic procedures to measure geometric tolerances with different machines while exploiting functionalities of advanced software such as Geomagic® Control X™ and PC-DMIS.

In Chapter 2 a literature survey is presented. Chapter 3 discusses the problem and its scope. Chapter 4 presents the methodology, and Chapter 5 discusses the results and conclusions.

CHAPTER 2: Literature Review

2. Summary

The literature survey begins with CMM the evolution of this equipment in metrology. The capabilities of accuracy are mentioned as well as studies carried out for flatness verifications to estimate the deviation using them. The second part of the literature review covers the sampling strategies that are used in the research Aligned Systematic, Halton-Zaremba, and Hammersley. These methods are commonly used in the verification of flatness and are described in detail. The constraints and equations that are used to calculate the coordinate points with each of these strategies are explained in detail. The last section refers to AACMM and the most important research studies done for this apparatus, covering the most studied subjects for this equipment. Calibration to reduce errors in measurement, kinematics and uncertainty are hot topics for these machines. A comparison of data measures with AACMM and CMM is not discussed or published in these studies.

2.1 Coordinate Measuring Machines

CMMs with computer control has been used in metrology since their creation in 1956. Then the manufacturing industry was converting into a more automated process. The biggest need at the time was an inspection process that consumed less time than gauges and blocks arrangement. After the industry discovered that these machines were reliable they became more popular (Robert & Paulo, 2011). Because of CMM's accuracy to 100 micrometers (μm) is possible to inspect parts with more precision, which is of high importance for the mating of parts and to produce parts from different sources. Keeping the same reliability is key for acceptance of the part and functionality of the final product.

The use of CMM has allowed inspection of complex parts. To achieve faster inspections sampling methods have been developed. To calculate the error fitting, algorithms have been refined to find the estimation of the error zone. Important advances have been done in providing guidelines to perform inspections using both mathematical models and a systematic process to verify the accuracy of the parts. (Aguirre Cruz, 2007).

Estimation of tolerance zone using search-based sampling for both straightness and flatness has been addressed by (Badar, Raman, Pulat, & Shehab, 2005) basic factors as part size, machining process, tolerance specification affect the sample size to represent the geometric feature.

Methods used to sample parts for flatness are hybrid search, tabu methods, and Hook-Jeeves sampling algorithms which are adaptative sampling methods saving the number of points optimizing the inspection of surfaces. (Obeidat & Raman, 2011) For verification of face milling and end milling pattern and experimental work on flatness. (M. Badar, Raman, & Pulat, 2005) Adaptative methods have been used in order to make a trade-off between benefit of additional sampling and cost increased time by using tabu search, Hooves-Jeeves and hybrid (a mix of tabu and Hooves-Jeeves search)(Badar, Raman, & Pulat, 2003) To select the number of points there are studies specifically for flatness and error is calculated with least-squares or minimum zone having a large sample number of 200 points for a surface area of $65mm \times 65mm$. (Raghunandan & Venkateswara Rao, 2008)

Alternate methods for sampling surfaces have been also studied by (Collins, Fay, Aguirre-Cruz, & Raman, 2007) in the case of spiral and Hampsi methods they usually have higher error in the corners because these patterns do not take those zones into account, for this reason, is important always to find a better sampling method that can represent more accurately the geometry.

Lastly, in today's Industry and shop floors CMM is not being used as frequently, being replaced by AACMM, although we still rely on higher accuracy taken with CMMs, the trend is moving to simpler metrology methods, taking even less time in the inspection tasks, without expert operators and providing real-time results, that can be used to make important changes that can avoid waste.

2.2 Sampling Methods

Sampling methods are used by selecting a representative part of the complete data. This data is then more manageable and will represent well enough the complete data. Sampling is used because it reduces time, cost and brings a higher scope. Regarding time, if there is no need of taking absolutely all the data, it means a reduction of time. When talking about the cost it is a combination of the resources consumed to take a sample compared with taking the whole data and having an accurate result. Lastly for scope due to the requirements to take the data, which may be specialized operators for special equipment it is a limited resource. Then, taking a survey of the

entire data is the best option. (Cochran, 1977). The variations in dimensional accuracy and surface finish are the ones which will determine the proper sampling size for the geometric feature that has been generated by the milling machine (rough pass) (Lee, 1997).

2.2.1 Sampling Strategy Aligned Systematic

This is considering a uniform sample method were using a random pair of numbers (Sukhatme & Sukhatme, 1970) (Kim & Raman, 2000). The column and row of strata are driven by the same interval and location. The arrangement of the points is made in zr rows and each row consists of xy units. Once the selection of a systematic sample of xz units is chosen, the procedure is as follows:

- Random selection of pair numbers (p, q) such that $p \leq r$ and $q \leq y$
- These numbers will establish the coordinates of the upper left unit by the qth unit in the pth row.
- The rows are calculated using the form

$$p, p + q, p + 2r, \dots, p + (z - 1)r \qquad (1)$$

- The columns are calculated using the form

$$q, q + y, q + 2y, \dots, q + (x - 1)y \qquad (2)$$

- The point where x selected rows and z selected columns to intersect is used to determine the xz select units
- N is the total number of sampling points

2.2.2 Sampling Strategy using Halton-Zaremba

From (Woo, Liang, Hsieh, & Lee, 1995) to calculate the coordinates with this sampling method there are some constraints that must be taken into account. The following are the equations to calculate the P and Q for the coordinates.

$$P_i = \frac{i}{N} \sum_{j=0}^{k-1} b_{ij} 2^{-(k-j)} \qquad (3)$$

$$Q_i = \sum_{j=0}^{k-1} b_{ij}' 2^{-(k-j)}$$

(4)

The definitions and restrictions of the variables are as follows:

- N is the number of sampling points $i \in I = [0, N-1]$ and it is constrained to be $2^k = 2, 4, \ldots$ for $k > 1$
- b_i = is the binary representation index i
- b_{ij} = is the jth bit in the b_i
- b_{ij}' = is $1 - b_{ij}$ for j odd, and b_{ij} otherwise
- $k = \log_2 N$

2.2.3 Sampling Strategy using Hammersley's Method

From (Lee, 1997) to calculate this strategy we require:

- Set $0 \leq s_i, t_i \leq 0$

To calculate the coordinates (s_i, t_i) of Hammersley point in two-dimensions can be simply determined as

$$s_i = \frac{i}{N}$$

(5)

$$t_i = \sum_{j=0}^{k-1} \left(\left\lfloor \frac{i}{2^j} \right\rfloor Mod2 \right) \times 2^{-j-1}$$

(6)

- N is the total number of points $i \in I = (0, \ldots, N-1)$
- $k = \lceil log_2 N \rceil$ is the smallest integer $\geq log_2 N$
- $\left\lfloor \frac{i}{2^j} \right\rfloor$ is the greatest integer $\leq \frac{i}{2^j}$

2.2.4 Error Calculation for Data Obtained with CMM

After the collection of data with the CMM, it is necessary to find a fitting criterion, it is also important to know that the method produces considerably different results when measuring a

workpiece with form error. Common fitting algorithms are the least-square methods and minimum zone. The most frequently used method in metrology, the method estimates regression coefficients minimizing the sum of squares errors in multiple regression method (Choi & Kurfess, 1999)(Montgomery, Rugner, & Hubele, 2011) Although computationally efficient in time to evaluate the data it overestimates the zone error due to its sensitivity to outliers

Conversely, minimum zone or min. max. evaluates geometric tolerances, this method's goal is to fit the collected data into a tolerance zone. It all the data is inside this zone it will be considered as accomplishing the specifications. The objective of this method is to minimize the maximum deviation, this provides a closer fit than least squares.

2.3 Articulated Arm Coordinate Measuring Machines

We found several researchers talking about the calibration of the AACMM, there are calibrations that might be of interested in the use of laser tracker given that it needs a periodic calibration before taking the measurements. For AACMM it has been thought the replacing of conventional one-dimensional gauges as ball bars by laser tracking (Acero et al., 2015). This is seen also using laser triangulation sensors (LTS) because of their versatility (Santolaria, Aguilar, Guillomía, & Cajal, 2011).

In general, it is seen that it is of much importance in research how an AACMM is calibrated so the error produced can be ignored and the level of uncertainty stays low. Because of the importance of producing accurate data that can be analyzed to draw conclusions in the measurement of geometric features we studied works on calibration and compensation techniques for AACMM, given that these machines are more trusted at shop floor than in laboratories because of the uncertainty levels that can reach, given its many axes, complex structure and gravity-induced deformation (Li, Chen, & Qiu, 2013).

Because of the rotating joints replacing the length measurement reference with an angle measurement reference, when compared to the Coordinate Measuring Machine (CMM) there are several advantages given its easy use, but this brings errors that need to be compensated (Luo, Liu, Li, & Tian, 2018). From the calibrations, it is possible to know the pros and cons of the AACMM in the market, such as limiting dimension and admissible error (Markov & Sharamkov, 2014).

From the state of the art, we found little information about uncertainty when measuring mechanical pieces, these papers are more related to the error that is found because of the

articulations, kinematic systems according to parameters in the axes x, y, and z of each of the joints that AACMM has (Markov & Sharamkov, 2014). Although this project is focused on the reading of one geometric feature in different stages of the life of a part, we require the calculation of error and uncertainty in the flatness measurement of the part against the perfect form (CAD model).

The inspection carried out on the rectangular block requires taking the data and using different features of a software that will process both the three parts through scan registration and taking of points with a probe on its upper surface, uploading these two images to Geomagic® Control X and using Alignment to start making this comparison and measurement through the software.

Although this equipment has improved from research stages to today's technology, the accuracy of non-contact devices is still lesser than the one of probing. The biggest advantage of scanners is to collect thousands of points in a considerable small amount of time. Still, factors as reflectance and shape can cause noise that represents error to the measurements (Cuesta, Rico, Fernández, Blanco, & Valiño, 2009). Uncertainty can increase due to additional sources of error in the methods used to take the survey. Improvement of acquisition of data with scan focuses on multiliteration, decreasing noise. (Aguado, Santolaria, Samper, & Aguilar, 2013)

error affecting the measurement uncertainty of the laser tracker, additional sources of error that further contributed to the uncertainty, and the factors influencing these techniques. We also define several noise reduction techniques for the measurements. The improvement in the accuracy of captured points focuses on a multilateration technique and its various resolution methods both analytically and geometrically. Similarly, we present trilateration and least-squares techniques that can be used for laser tracker self-calibration, which is an essential parameter in

The registering of data depends of course of a skilled person that does not generate noise that can generate a high error and uncertainty levels ("Webinars | 3D Systems," 2019)

This research then is concerned with how the changes in geometrical features can be measured, concentrating on the flatness of the top surface and how the FARO arm is capable of finding these differences as a deviation from measured data to perfect form. These results are of important interest in developing new methods for designing, decision-making factors for manufacturing processes used in the fabrication and quality control of the part. This is important

because it will save time, consequently money and it shows a systematic process for the adequate management of the data and how to compare it.

CHAPTER 3: Problem Definition

3. Problem scope

In this section, the scope of the problem is described, as to what was done and what is still future work to do, where this research will be effective, and how it is innovative. Flatness is the geometric feature used to compare the capabilities of two measuring instruments. Methods for analyzing points obtained from sampling using a CMM (Browne & Sharpe Gantry type) and a scanning cloud of points obtained using an articulated arm (FaroArm® using Geomagic® Control X™) is developed. It is shown how the measured data from different machined surfaces deviate in flatness from the perfect form, through data collected with the two instruments.

Figure 2 describes the procedure employed for measuring surfaces manufactured by rough and finish passes. An AACMM FaroArm® Platinum with laser ScanArm® is used to measure the flatness feature of the top surface of such manufactured parts. The CMM is also used using several sampling schemes for measuring discrete points from the same surfaces. An inspection for flatness was thus carried out for the six samples, collecting data using CMM and AACMM. These are compared to the theoretical part designed using CAD. The comparison of the actual points versus theoretical points allows for obtaining flatness deviation. After flatness verification, the scanned data and points for each sampling method were compared obtaining a distribution of the points and a fitting for both measurements.

There is no evidence in the literature of such a comparison of measurements using CMM and AACMM. All the same, it is important for AACMM to be developed as a viable alternative to CMMs in the inspection verification of parts.

In future work, it is possible to compare measurements of more complex geometries using this equipment to further develop AACMM as metrology equipment.
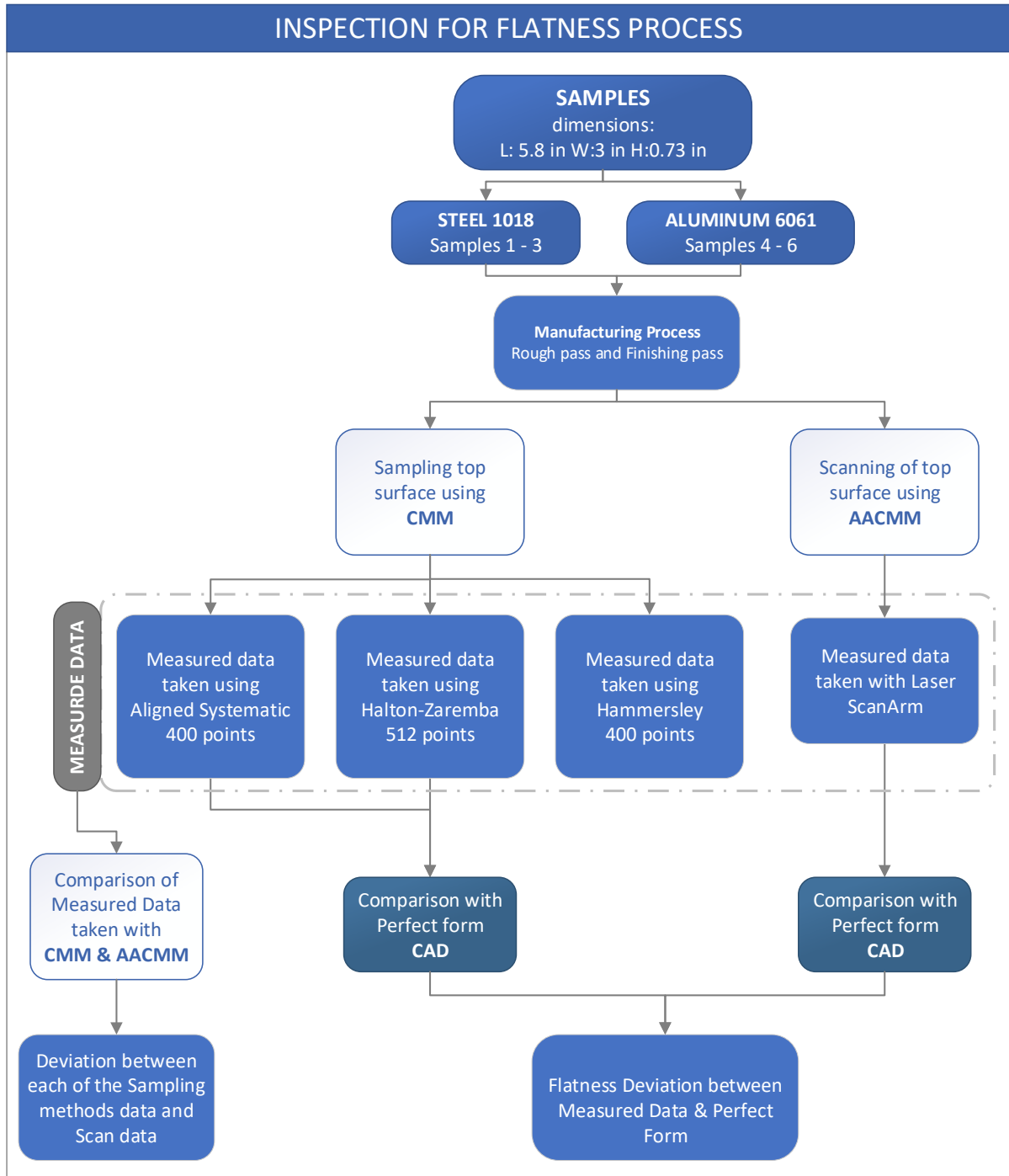
Figure 2. Flatness Verification and Measure Data Inspection

CHAPTER 4: Methodology

4. Summary

For this research as mentioned previously, we will focus on measuring the flatness of the top surface of the six samples that are all rectangular blocks. Steel and aluminum were the two rectangular blocks used in this research (purchased from Online Metals). These parts were machined at the Rawl Engineering Practice Facility (REPF) of the University of Oklahoma (OU) using a Summit VS-350 Mill. The samples have approximate dimensions (length) 5.8 in, (width) 3 in and (height) 0.73 in. The first three labeled samples are of Steel 1018 and the next three are of Aluminum 6061. *Figure 3* summarizes the processing of the six sample parts from the raw material.

Raw material **-Steel 1018 and Aluminum 6061**
Original dimensions: L 25 in X W 3 in X H 0.75 in

Cut raw material in three rectangles
dimension: L 5.8 in X W 3 in X H 0.75 in
Using Horizontal Bandsaw

ROUGH PASS
using milling Machine taking 0.02 in from top surface
CAD dimensions: L 5.8 in X W 3 in X H 0.73 in

FINISH PASS
using milling Machine taking 0.06 in from top surface
CAD dimensions: L 5.8 in X W 3 in X H 0.67 in

Figure 3. Flowchart of the Manufacturing Processes for the Parts

The top surface of the workpieces went through a rough pass using a $3/4 \times 3/4$ HSS flute single-ended mill tool with a spindle speed of 1,000 r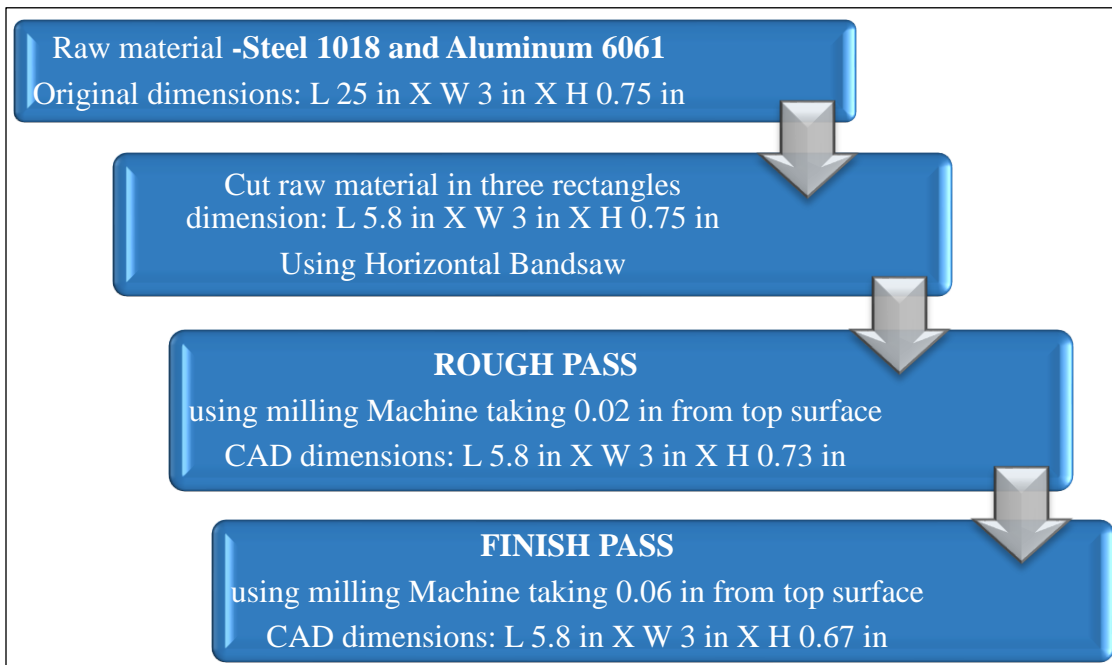pm and depth of cut of 0.01 in. Two passes were made to take 0.02 in from the initial height and another part with a height of 0.73in was made. A surface pattern was visible to the naked eye, due to the coarseness of the finish left by roughing. Flatness was verified after the rough pass using CMM and AACMM for the six workpieces collecting six measurements for the scan data and eighteen measurements for the sampling of the scanned data.

For the finish pass, the tool used was a four tipped indexable square-shoulder face milling tool using 60º inserts of carbide TCMT 32.52 CM14, the spindle speed was 300 rpm and depth of cut was 0.01inch in making 6 passes to obtain a part with a final height of 0.67 in. This process is expected to leave a smoother surface than with rough machining.

Flatness was verified by measuring the difference in the (X, Y, Z) components of the coordinates of CMM sampling points with respect to the perfect form, and the comparison is made inside the form tolerance zone that ranges from parallel planes -0.002 to 0.002 in. Similarly, the cloud of points obtained from the scanner compares the gap between each component of the coordinate and does a calculation to find the deviation of flatness.

The collected points were stored and processed in a Dell® Precision 7720 laptop computer with Intel® Core™ i-7. The data obtained from the Python™ was processed using Microsoft® Excel 2016 and a macro is shown in APPENDIX E to obtain .txt files that can be uploaded on Geomagic® Control X™ Software.

4.1 Perfect Form

To have a reference for comparison, a theoretical part is constructed using Computer Aided Design (CAD) software Solidworks®. A rectangular block of dimensions 3 in wide, 5.8 in long and 0.73 in high was modeled, as in *Figure 4* to compare with parts made by a rough pass. This CAD part is necessary for Geomagric® Control X™ to perform the fitting of the geometric feature and compare the measured data either by scan or sampling method. Figure 9*Figure 5* corresponds to the CAD model of dimensions 3 in width, 5.8 in length and 0.67 in height used for comparison of parts made by the finish pass.
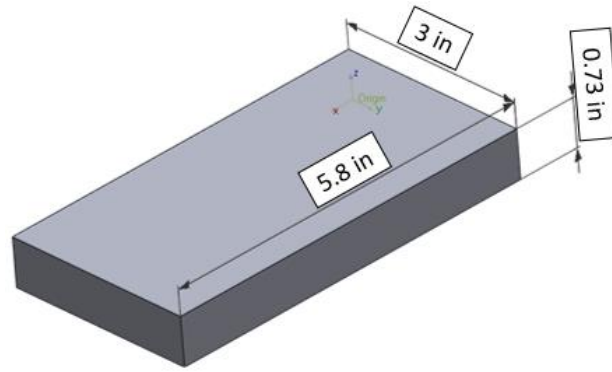
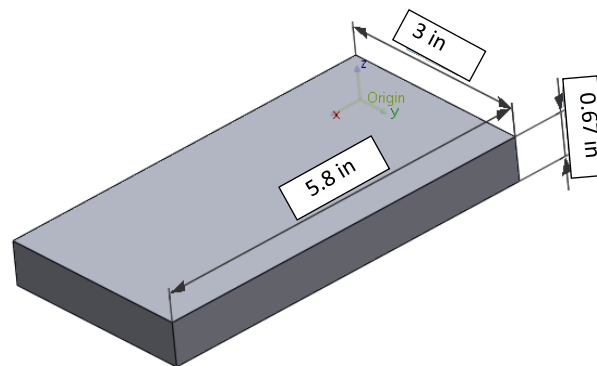*Figure 4. CAD Generated Perfect Shape for Face Milling Rough Pass*

Figure 5. CAD Generated Perfect Shape for Face Milling Rough Pass

4.2 Flatness

Flatness tolerance is the zone between two parallel planes within which all points of a given measured plane may lie. For this research, the tolerance is limited between two planes ±0.002in creating a zone of 0.004in where the data may deviate with the perfect shape. This tolerance was set according to typical milling dimensional tolerances.

To measure the flatness, we are interested in showing the gap from the coordinate components points (X, Y, Z) and how they vary from the perfect shape. This difference will show how much the flatness of the sampling points obtained with CMM or cloud of points obtained with AACMM deviates from the perfect form. *Figure 6* displays the points of the perfect shape, although there is a tolerance zone all points are in one plane and do not deviate from it. The theoretic part shows then that it does not have any flatness deviation.
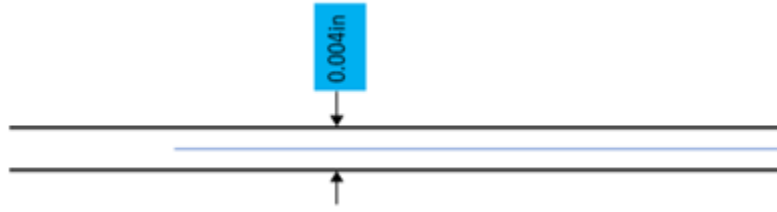
Figure 6. Flatness Tolerance for Perfect Shape

Figure 7 illustrates the parallel planes that are the form tolerance for flatness, the cloud of points obtained with the laser probe is in a profile view to show how some of the points are out of the tolerance form. Those points that are out are to be considered the flatness deviation.

Figure 7. Flatness Tolerance for Scan data

For *Figure 8* it is possible to see how sampling points go inside and out of the tolerance zone. Points inside are consider fitting to perfect form were as points outside are to be the deviation.

Figure 8. Flatness Tolerance for Sampling data

4.3 Experimental Procedures and Apparatus

The experiments for this research were executed in precision metrology laboratory located in Carson Engineering Center room CEC33 with a temperature of 65 degrees F, for the me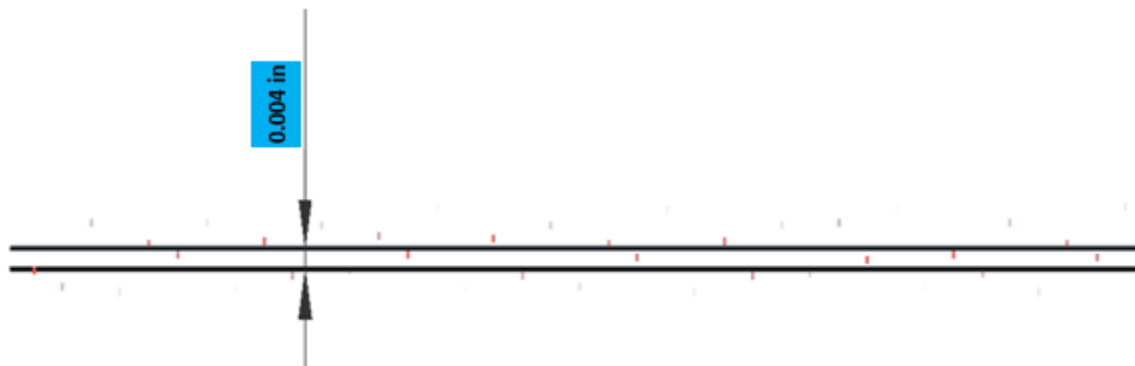asurements with CMM. For measurements with FaroArm®, the experiments were carried out in an ultraprecision metrology laboratory located in CEC24 at the same temperature conditions.

4.4 Coordinate Measuring Machine: Brown & Sharpe Microval PFx™ 454

The CMM used for the inspection of the rectangular blocks is a Brown & Sharpe Microval PFx™ 454, its specifications can be found in

APPENDIX B. The software to process the data for this machine is PC-DMIS™, marketed by Hexagon manufacturing intelligence. Algorithms for this program are proprietary and employ least squares for computing form tolerances.

A Renishaw® tip with Ruby ball/stainless steel stem A-5000-3554 was used to probe the surface of the blocks. The dimensions of the probe are length 31mm (1.22in) and the tip is a ball tip of a diameter of 4mm (0.16in). ("Technical specifications: Styli and accessories (pdf)," 2016).

For inspection, it is important to first start with the calibration of the apparatus. The calibration was carried out verifying a standard sphere and obtaining a Standard Deviation result of 0.0001 in. Once calibration was done it was necessary to do an initial alignment probing a plane (three points) for Z, a vector (two points) for X and one point for Y to find the origin of the part.

The following steps were to test the top surface of the parts using each of the three sampling methods to inspect the six pieces. Once the program has the points loaded the program was run to acquire the actual data from the part as shown in *Figure* 9.
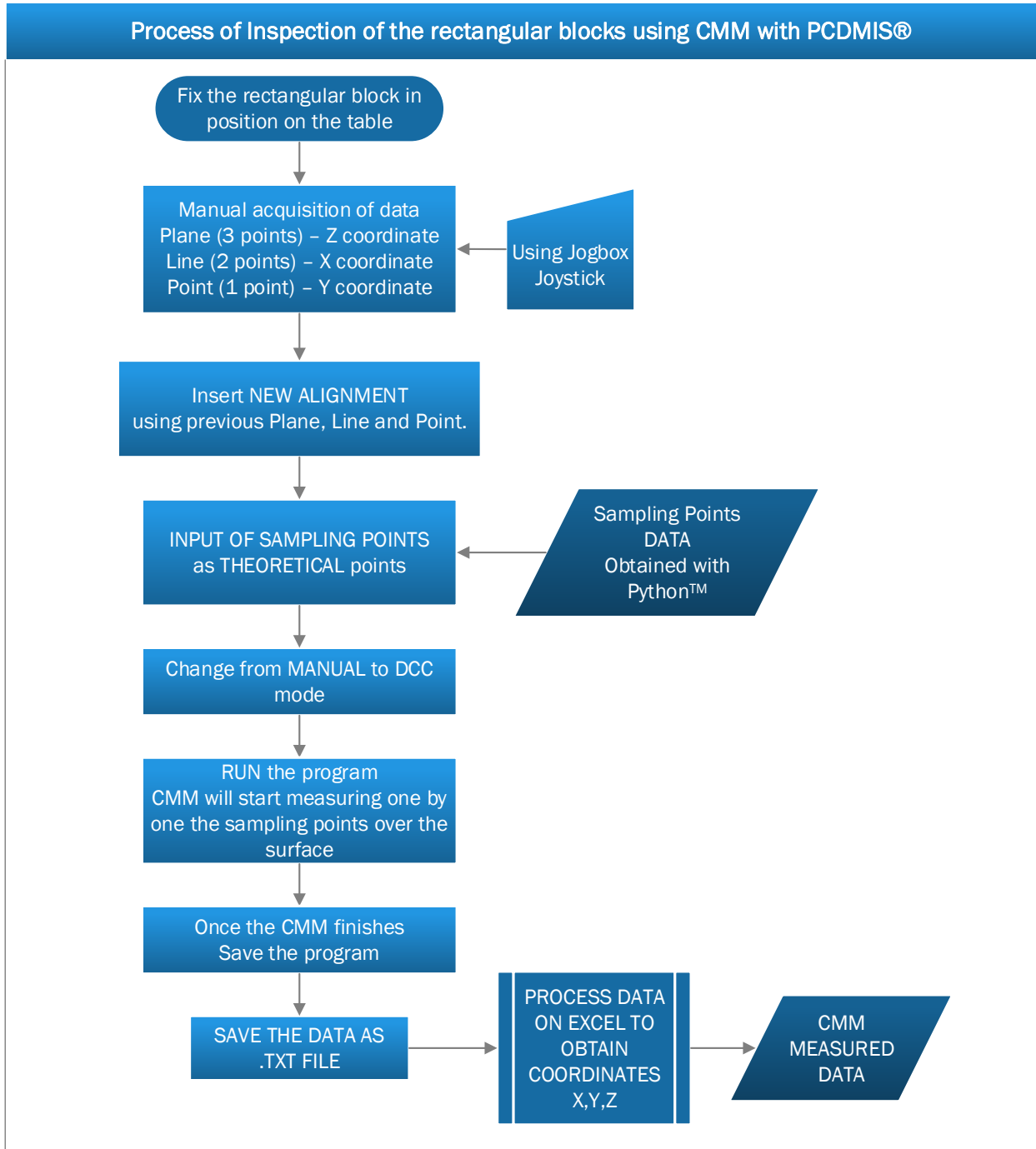
Figure 9. Process of Inspection using PC-DMIS® with CMM

4.4.1 Sampling Methods using CMM

To select the sampling methods there are several factors that must be accounted for: the required geometry, the geometric feature to represent and the machining parameters. (Badar & Singhal, 2006). To select the sampling survey, we researched for the most used for flatness

representation. We selected three sampling sequences that are more frequently used for flatness Halton-Zaremba (Woo et al., 1995), Hammersley (Lee, 1997) and aligned systematic (Kim & Raman, 2000). The sampling size was based on the dimensions of the blocks, as suggested by (Raghunandan & Rao, 2007) there is an allowance of 3 mm (0.11811 in) between points in the inspection zone, and for a sample of 2.6 in x 2.6 in a good size to represent the sample is 200 points. Another source to determine size was (Jalid, Hariri, & Laghzale, 2015) which suggests a lesser number of points to represent flatness, that a greater number of points create more uncertainty to measure flatness. The sampling sizes we choose are for aligned systematic N=400 points, for Halton=Zaremba we choose N=512 according to the constraints for the sample size and for Hammersley we choose a sample size N=400 points.

To generate the sampling coordinates, we wrote code in Python™ following the equations to calculate them that we mentioned previously in the literature in section 2.2 Sampling methods.

In the following section, we present these calculations and patterns generated for the CMM to measure over the top surface of the rectangular blocks. The sampling methods were carried out using PC DMIS™, this software allows to show the path for the probing and also to optimize this path. When the optimization is done the program performs the sampling reducing the time that it takes to it to survey the surface.

4.4.2 Aligned Systematic

The number of points was determined $N = 400$, two random numbers p and q were generated on Python™ the code can be seen in APPENDIX A using equations (1) and (2). The number of columns selected was $x = 40$ and rows $z = 10$. On *Figure 10* you can see the pattern formed to measure the rectangular blocks.
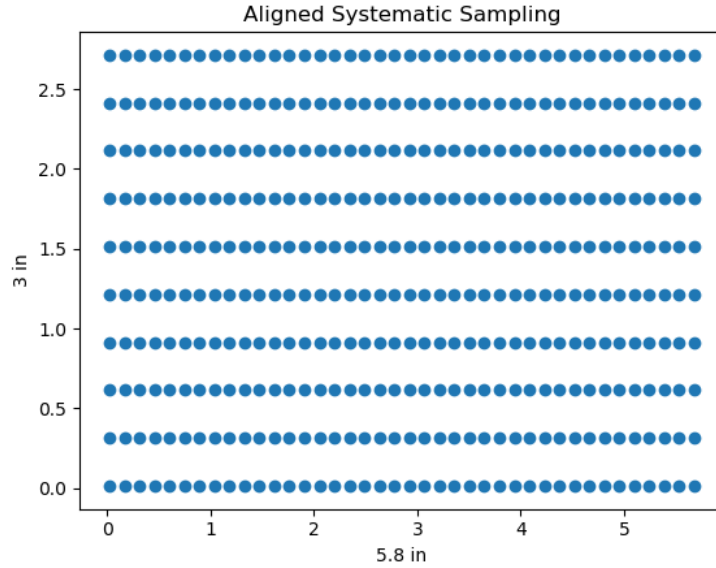
Figure 10. Aligned Systematic Sampling Pattern on Area 5.8in×3in

With the sampling we obtained (X, Y) coordinates, so to have a Z coordinate we add a constant number Z=0.70 in so the tip will try to go down to that height until it finds the real one. Coordinates should be converted from polar to Cartesian coordinates.

4.4.3   Halton-Zaremba

The size of the sample was determined as $N = 2^k$ with $k = 9$ then $N = 2^9 = 512$ points. Values p and q were calculated using equations (3) and (4) with a Python™ code shown in APPENDIX A. *Figure 11* shows the pattern of points obtained for this sampling strategy. The coordinates obtained are polar coordinates, that should be transformed to Cartesian coordinates to cover completely the surface of the blocks. For height coordinate Z we determined a constant number $0.70\ in$.
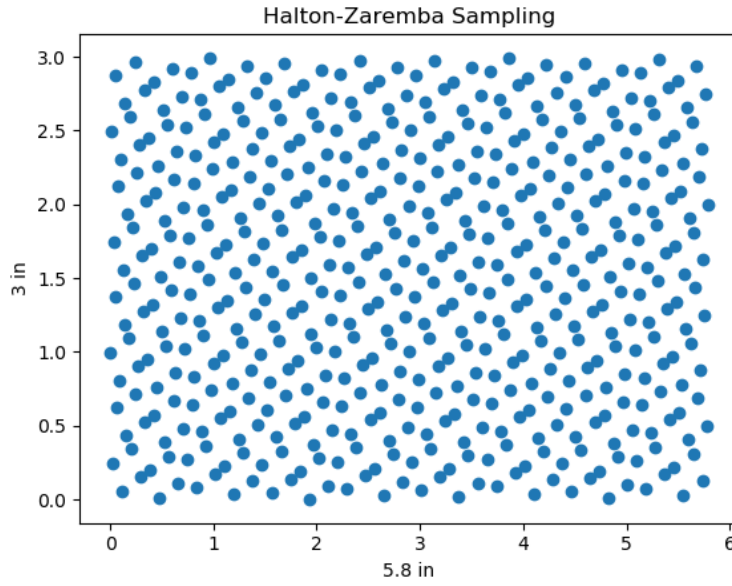
Figure 11. Halton-Zaremba Sampling Pattern on Area 5.8in×3in

4.4.4   Hammersley

The number of points for this method was $N = 400$, to calculate s and t we used equations (5) and (6) respectively using Python™ the code can be found in APPENDIX A. The coordinates obtained were converted from polar to Cartesian. Height for the coordinates is set as a constant of $Z = 0.70\ in$. The pattern obtained with Hammersley is shown in *Figure 12*.
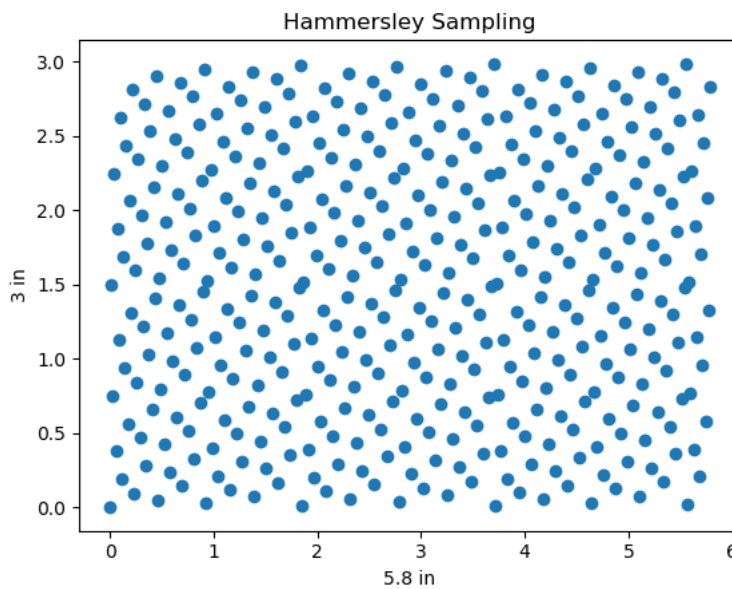

Figure 12 Hammersley Sampling Pattern on Area 5.8in×3in

4.4.5   PC-DMIS Sampling

Once the data for each of the sampling was uploaded into PC-DMIS it is possible to see the path lines in green generated by the software, this path goes along the points in numerical order. To optimize this path the software has a feature called optimize path, the program will ask from which point on the optimization will start. For the three sampling strategies, the optimization started from point 2, this is because point 1 is used for the alignment. Once the point is selected the program presents the percentage that will optimize for the line path as shown in *Table 2*. This allows the sampling to be faster in the surveying of the top surface. Each image shows a small triangle accountable for the plane (three points) axis Z, a line can be seen in some of the images for the vector (2 lines) axis Y and the path for axis Y. These combinations are used for the origin shown in red and green are the arrows representing the axes.

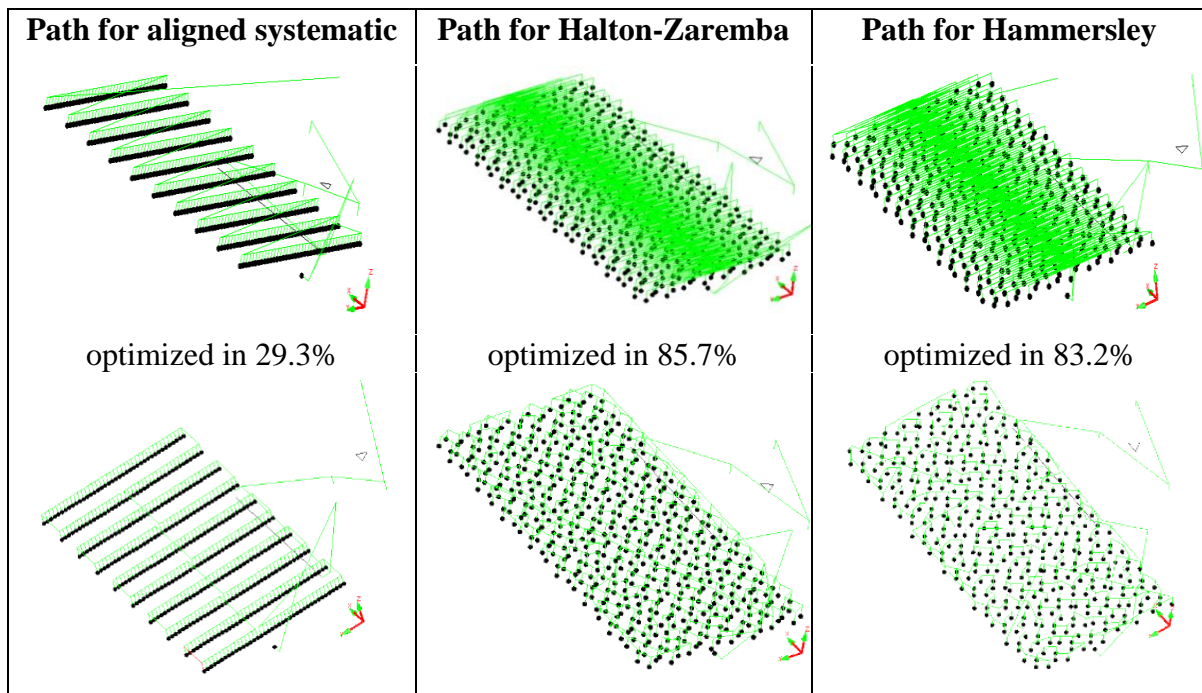| Path for aligned systematic	Path for Halton-Zaremba	Path for Hammersley
optimized in 29.3%	optimized in 85.7%	optimized in 83.2%

Table 2. Path Optimization According to Sampling Method

4.5 Articulated Arm Coordinate Measuring Machine: FaroArm Platinum with Laser ScanArm

The AACMM used for inspection is a FaroArm® Platinum, and its specifications can be found in

APPENDIX B. The software used is Geomagic® Control X™, marketed by 3D Systems, and has proprietary algorithms for calculation of deviation of geometry from measured data and reference data.

For collecting data, there were two probes used, a contact probe A-5003-7673 zirconia ball with diameter 3mm (0.11811in) ("Technical specifications: Styli and accessories (pdf)," 2016) to take the points for alignment. A plane (three points) to set on Z-axis, a vector (two points) to set X-axis and position (one point) to define the origin and Y-axis. The other probe used was a non-contact probe. The equipment uses a laser line probe or not-contact probe V3 Laser Line Probe. For calibration of the laser probe, there is a process that must be followed to pass. Calibration of ball probes and plane probe are required for a correct collection of data.

After calibration is performed collection of data by swiping the laser probe over the surface is done. The raw scan then needs to be processed for taking extra scanning that is not from the top surface to avoid having erroneous data. When the data is clean the process illustrated in *Figure 13* can be followed to process the data to first find the flatness deviation against the perfect form. And second, to compare the data measured in CMM with the scan data.

Scanning with FaroArm® although easier represents a challenge with material shininess and scanner itself. It is necessary to have good practice when using the scan to record the surface to avoid creating imperfections like holes, collection of data needs to be done with a smooth technique that prevents irregularities to appear on the scan due to fast movements. *Figure 13* illustrates the process of inspection using FaroArm® ScanArm® and Geomagic® Control X™.
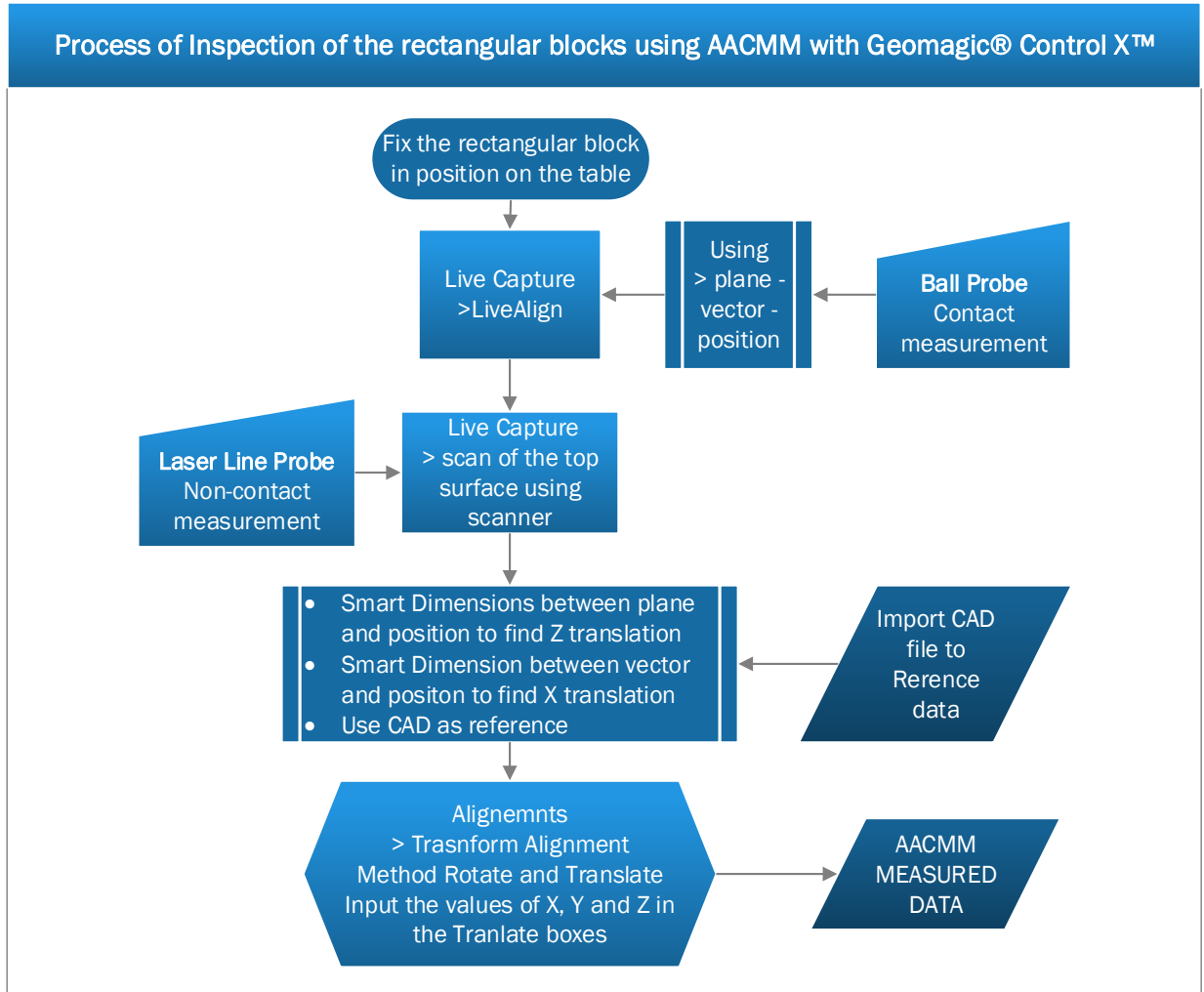
Process of Inspection of the rectangular blocks using AACMM with Geomagic® Control X™

Fix the rectangular block in position on the table

↓

Live Capture >LiveAlign ← Using > plane - vector - position ← **Ball Probe** Contact measurement

↓

Laser Line Probe Non-contact measurement → Live Capture > scan of the top surface using scanner

↓

- Smart Dimensions between plane and position to find Z translation
- Smart Dimension between vector and positon to find X translation
- Use CAD as reference

← Import CAD file to Rerence data

↓

Alignemnts > Trasnform Alignment Method Rotate and Translate Input the values of X, Y and Z in the Tranlate boxes → AACMM MEASURED DATA

Figure 13. Process of Inspection Using Geomagic® Control X^{TM}

4.5.1 Collection of data with AACMM

FaroArm® Platinum has two different approaches to collect data. Contact ball probe and non-contact laser probe. For this research, a ball contact probe of 3mm (0.12in) of diameter was used to acquire the data to make the Live alignment and a laser ScanArm® V3 to scan the top surface of the rectangular blocks that underwent rough and finish pass with a milling machine.

Probed points obtained with the ball probe for live alignment were translated to compensate the diameter of the probe to obtain the real (0,0,0) coordinate for each of the parts. The scan collection of data required the fixing of the part to the table, an appropriate distance of the laser probe to the surface and soft swipes to obtain data that represent well the geometric feature and avoid noise on it.

25

4.6 Flatness Deviation

As mentioned, when defining flatness in section 4.1, to measure the deviation we use the form tolerance or two parallel planes that contain the points. Parallel planes for this research are 0.002 in. under and above the perfect top surface. Points obtained from the sampling method with coordinate components (X, Y, Z) obtain actual values, we are interested in how Z values change with respect to the perfect shape in the -0.002 to 0.002 in flatness form tolerance. For the data scanned the software captures clouds of points that contain vector for the position (X, Y, Z) and find the gap between the cloud of points and the perfect shape. *Figure 14* shows in a graphic flow how the data is processed using Geomagic® Control X™ to verify flatness (Systems, 2018).
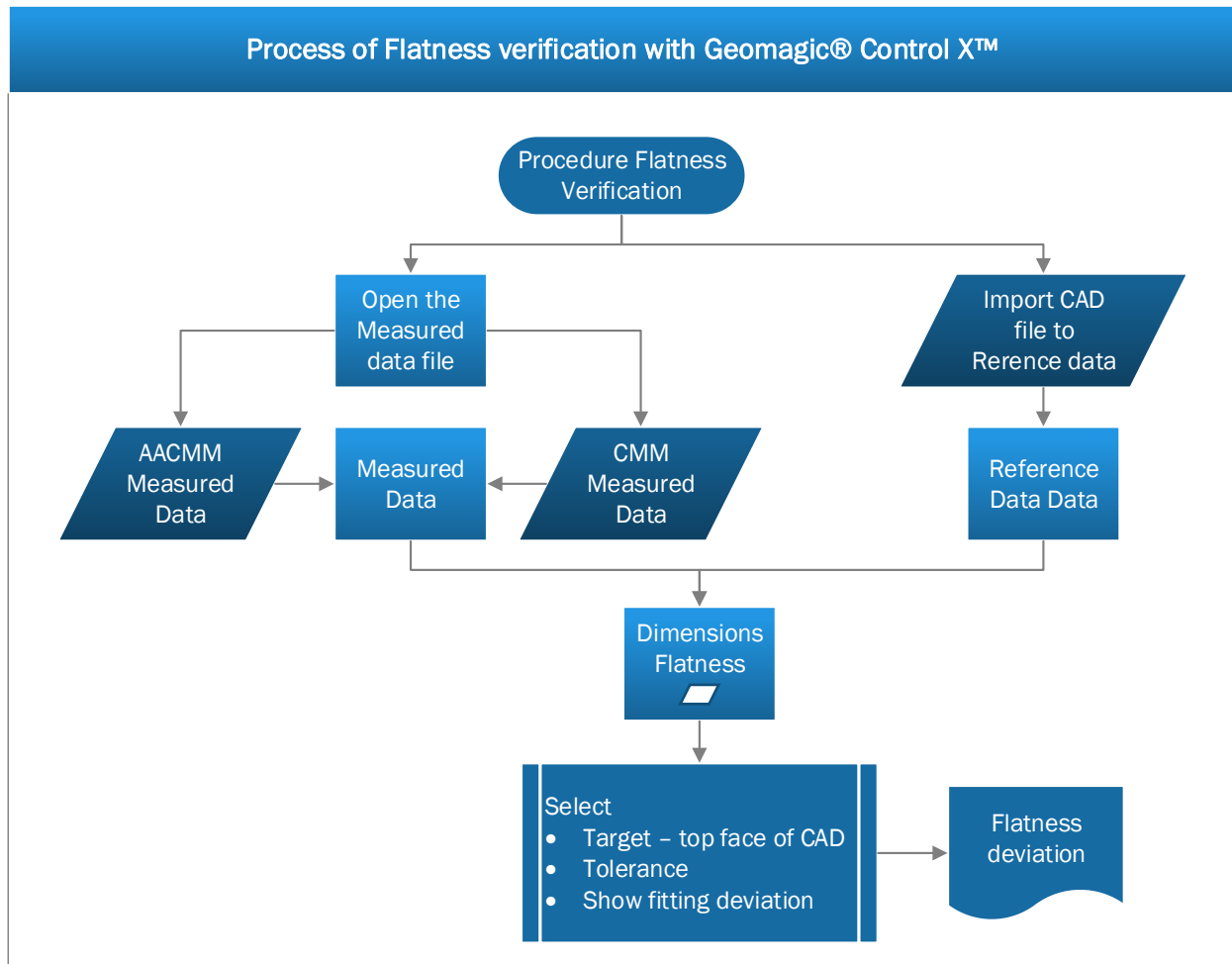

Figure 14. Flatness Verification Process

4.7 Comparison of Measured data

A complete methodology was developed to compare the data collected with the three selected sampling strategies. *Figure 15* explains the flow of steps that must be taken in order to accomplish a successful flatness verification and comparison of measured data. It is necessary to capture the geometric feature using each of the equipment. With AACMM the feature is scanned, and with the CMM the features are sampled using the strategies to represent the feature.

Measured data obtained with the FaroArm® requires a transformation of the alignment to correct the size of the probe ball and find the origin coordinate to assure that the measurements are correct. On the other hand, the measured data obtained with Brown & Sharpe PFx 454 CMM requires an initial alignment as well that to find the coordinate origin. Using Geomagic® control X™ the scanned data is transformed into a mesh. This conversion allows the data to be moved as reference data and later be compared with the sampling points that are imported as measured data. The 3D Compare function of the software requires to set tolerance and range, for our case it was ±0.002 in and ±0.005 in respectively.
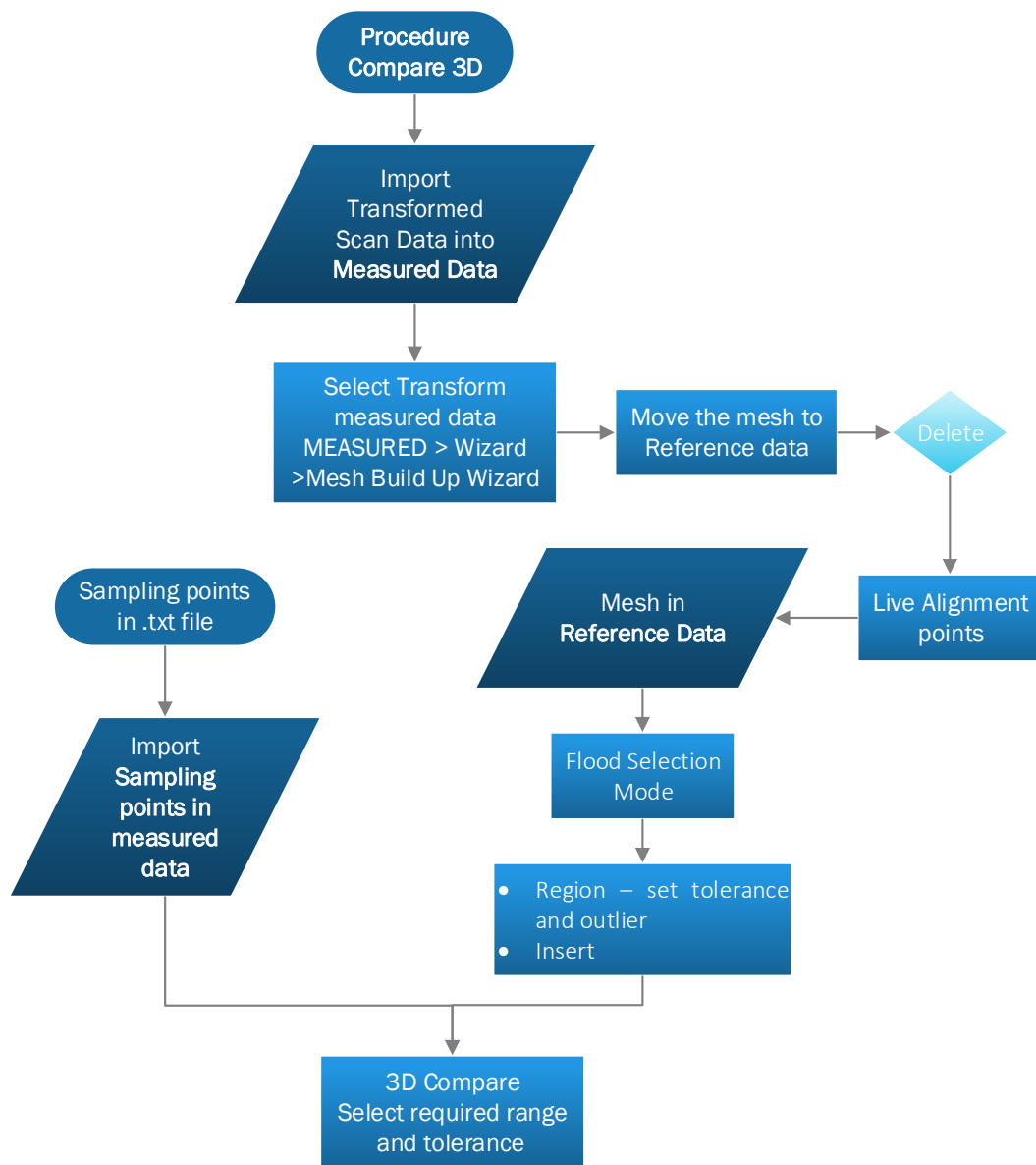
Figure 15 Flow Diagram of Flatness Verification and Measured Data Comparison

CHAPTER 5: Results and Discussion

5. Summary

The results are divided into two sections, the first one addresses the flatness deviation from the perfect form, for face milled rough and finish surfaces. The comparison is made between the data measured with the scan arm, and those obtained from the CMM with the sampling techniques employed, for each of the two passes against the theoretical form. The second section presents a comparison of the difference between the measured data obtained by CMM and AACMM. The deviation from these two measurements shows how significant the deviation of flatness representation in each sample is.

With these results, we expect to determine factors that could affect the measurements. How the sampling techniques can be effective in describing a geometric feature, and their weaknesses will be identified. More importantly, this research attempts to determine if the AACMM can be used as a viable alternative to CMM in geometry verification of manufactured parts. This could be of much importance to the industry in product inspection.

5.1 Flatness deviation

As mentioned before, flatness deviation concerns the points that are contained between two parallel planes forming flatness tolerance. The tolerance used is of 0.002 in, and that allows a zone of 0.004in within which the points that represent the flatness must lie.

5.1.1   Rough Pass

As an example of the results obtained using Geomagic® Control X™, *Figure 16* for Sample#1 (Steel 1018) shows the effect of the manufacturing process on the AACMM scan data and the points sampled with CMM using the three different strategies. Each of the measured data was compared with the perfect form. In the tag the actual value represents the deviation of flatness for the part and the number next to the flatness symbol is the tolerance given, the color convention is green presenting the best fit, and red the most deviant from the perfect form.

In *Figure 17* the measured data is presented for Aluminum 6061. This time due to a more ductile material the passes are much more noticeable than the ones on the steel, and so this

fingerprint creates higher deviations from the CAD part. The data obtained using Geomagic®
Control X™ is compiled in *Table 3* and displays the flatness deviation of the six sample rectangular
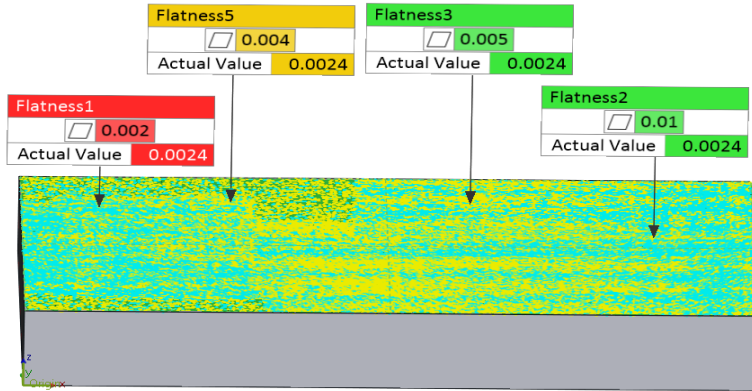blocks. The deviation is from the perfect part CAD.

Flatness Deviation for Rough pass obtained with Geomagic® Control X™					
Material	Samples	AACMM FaroArm® Platinum	CMM Brown &Sharpe MicroVal PFx™ 454		
		Scan (in)	Aligned Systematic (in)	Halton-Zaremba (in)	Hammersley (in)
Steel 1018	1	0.0024	0.0011	0.0055	0.0011
	2	0.0023	0.0007	0.0009	0.0009
	3	0.0025	0.0011	0.0010	0.0011
Aluminum 6061	4	0.0072	0.0050	0.0057	0.0054
	5	0.0084	0.0058	0.0059	0.0061
	6	0.0073	0.0054	0.0055	0.0055

Table 3. Flatness Deviation of Measured Data vs. Perfect Form for Rough Pass

In *Figure 18* it is possible to see the graph for the deviation values and make a comparison
where the CMM is the less deviated from the CAD. This is because of the better accuracy of
CMMs. Although the measurements are better, the Scan data is not too far from the coordinate
data. There is also evidence in Sample#1 that due to points taken on the edges the deviation can
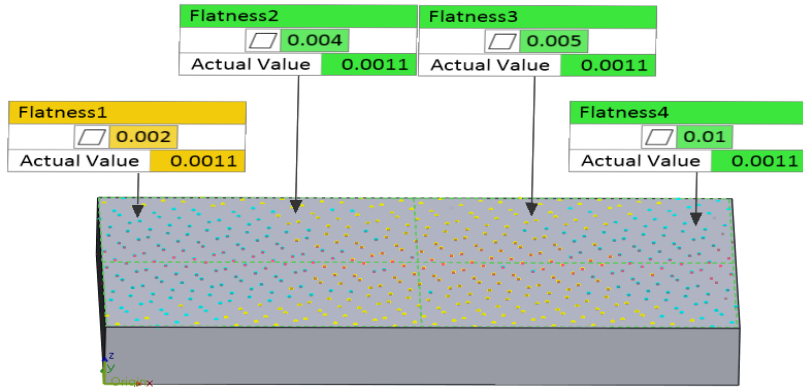increase considerably.
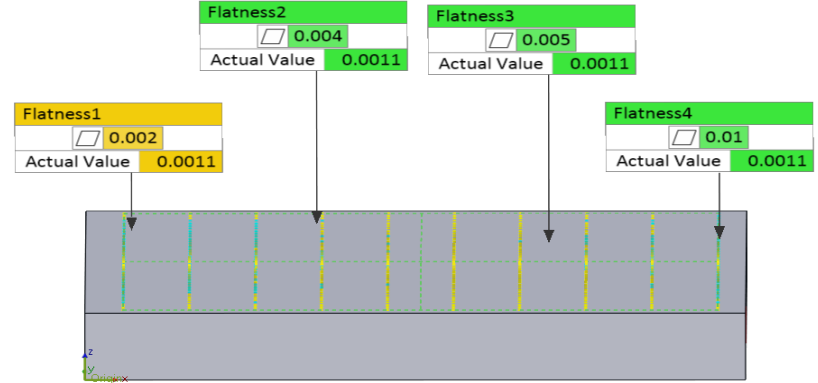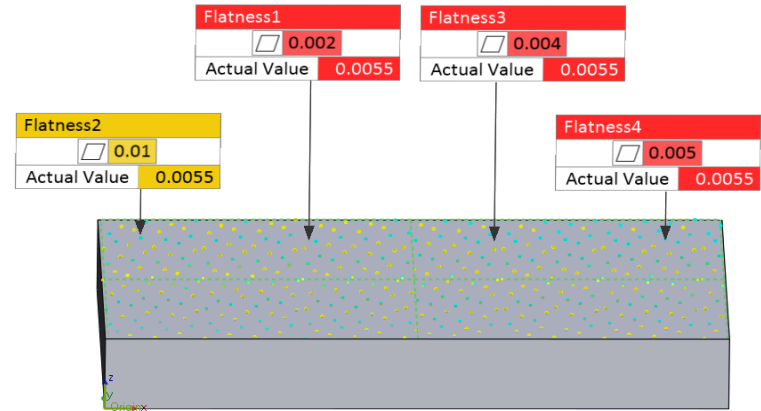
Figure 16. Sample #1 Flatness Deviation Measured Data vs. CAD Rough Pass
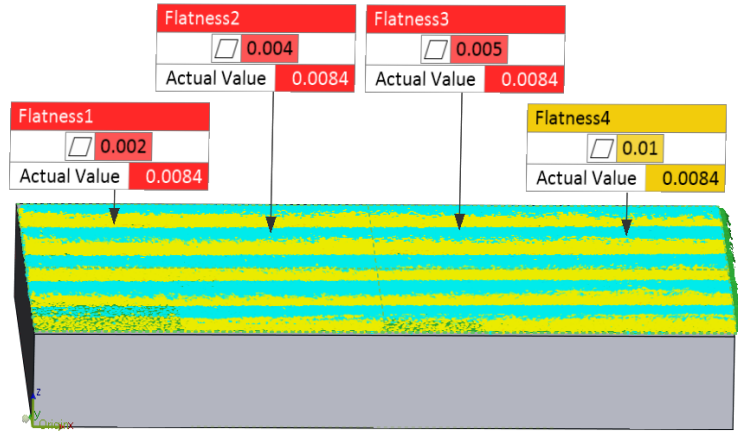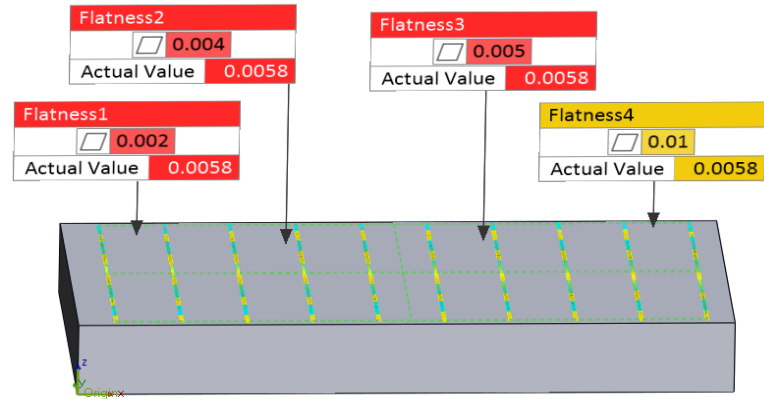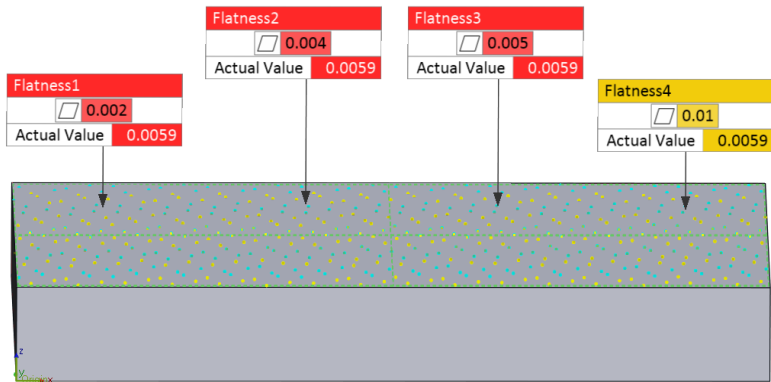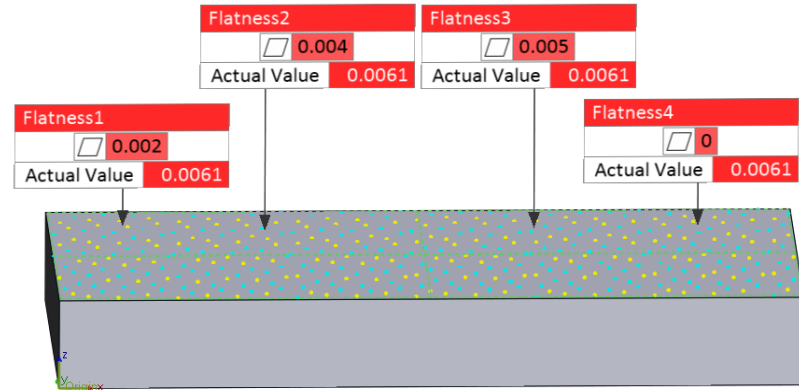
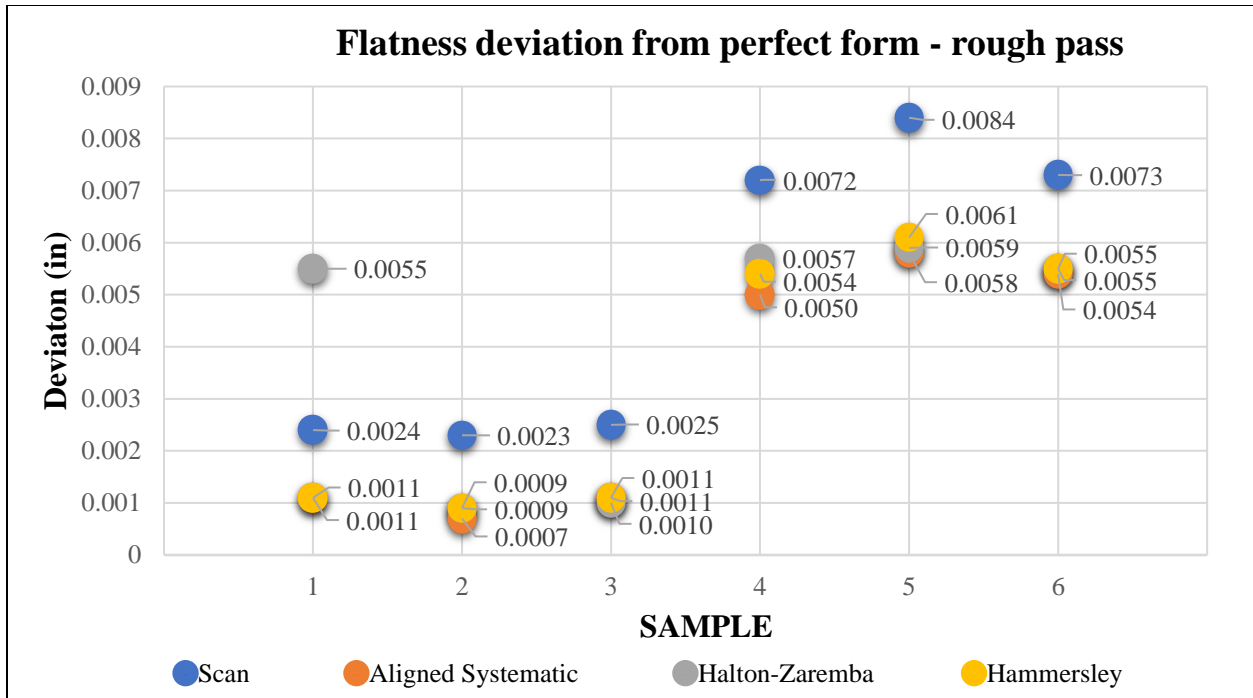*Figure 17 Sample#5* Flatness Deviation Measured Data vs. CAD Rough Pass

Figure 18 Flatness Deviation Measured Data Collected with AACMM & CMM vs. CAD – Rough Pass

5.1.2 Finish Pass

Figure 20 shows the results obtained with Geomagic® Control X™ for the (sample#2) Steel 1018, showing for the scan data a depression zone in the center due to the manufacturing process. The sampling data probed with CMM shows the fitting of the sampling points. All this data is compared against the perfect form. *Figure 21* is for sample#6 AL6061, and because of the ductility of this material, the passes are detected to have a depression in the middle, although the deviation is not as noticeable to the naked eye. *Table 4* shows the flatness deviation in inches for the six samples, the three sampling methods, and the scanned data.

Flatness Deviation for Finish pass obtained with Geomagic® Control X™					
		AACMM FaroArm® Platinum	CMM Brown & Sharpe MicroVal PFx™ 454		
Material	Samples	Scan (in)	Aligned Systematic (in)	Halton-Zaremba (in)	Hammersley (in)
Steel 1018	1	0.0078	0.0048	0.0052	0.0054
	2	0.0153	0.0114	0.0120	0.0130
	3	0.0184	0.0126	0.0129	0.0129
Aluminum 6061	4	0.0161	0.0111	0.0111	0.0111
	5	0.0165	0.0117	0.0114	0.0114
	6	0.0172	0.0117	0.0118	0.0118

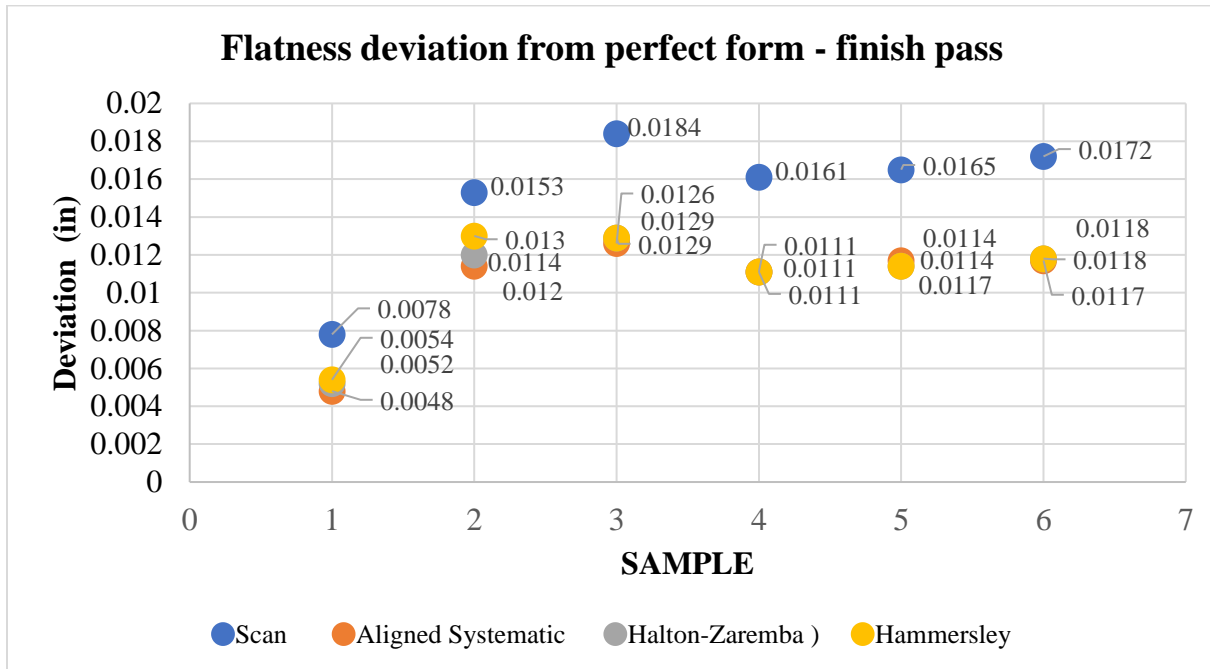*Table 4. Finish Pass Flatness Deviation of Measured Data vs. Perfect Form*

Figure 19. Flatness Deviation Measured Data collected with AACMM & CMM vs. CAD - Finish Pass
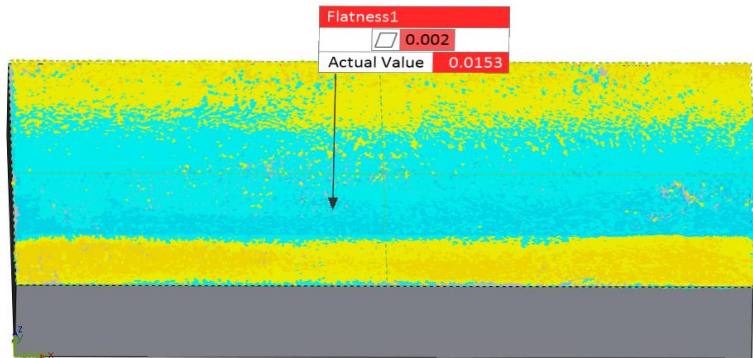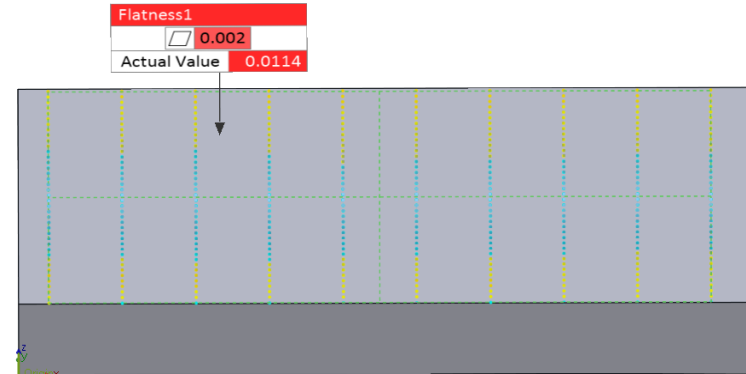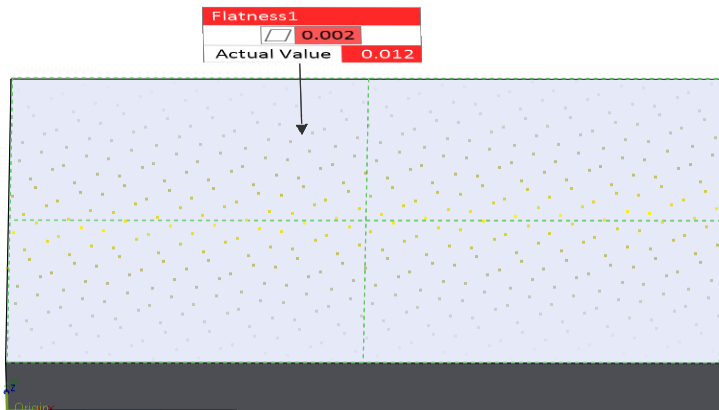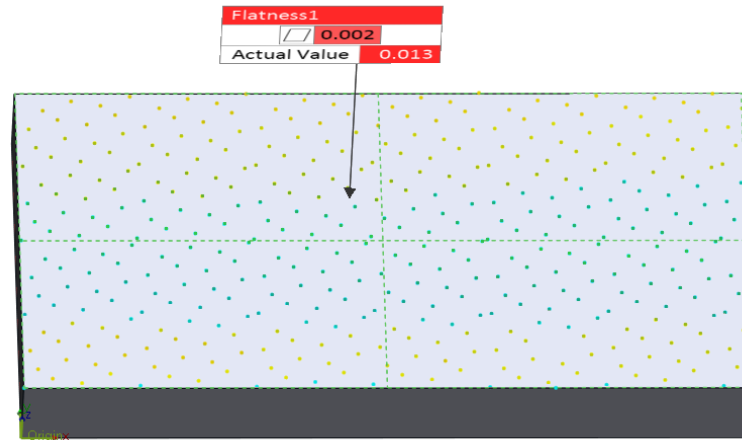
Figure 20. Sample #2 Flatness Deviation Measured Data vs CAD Finish Pass
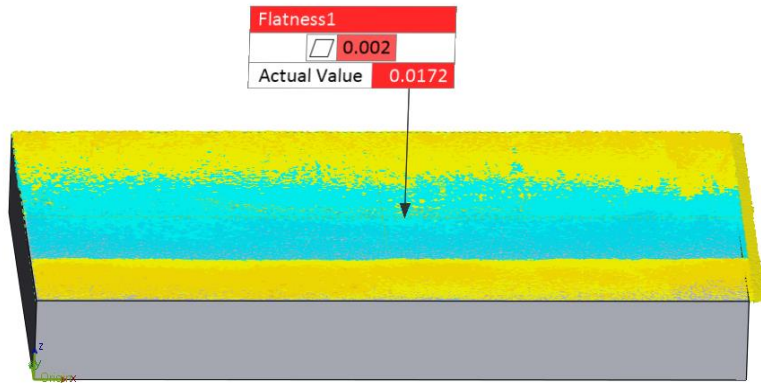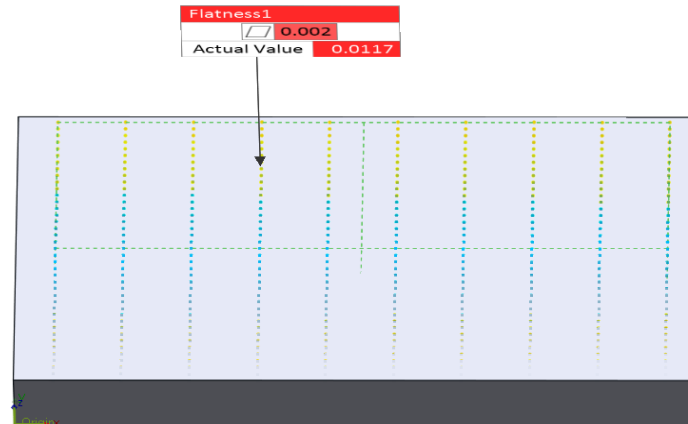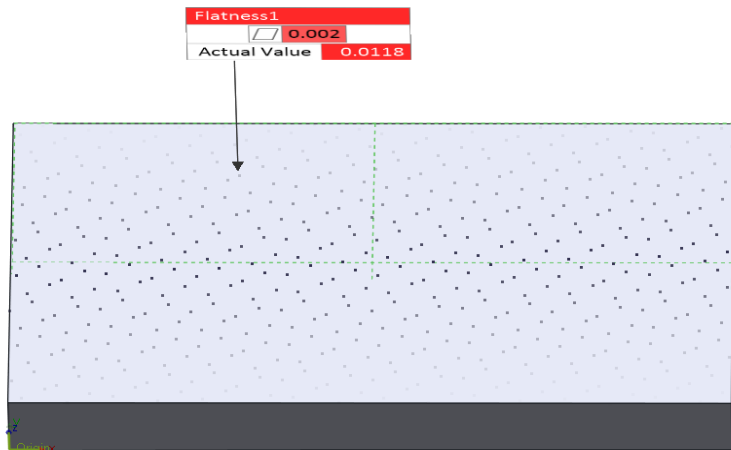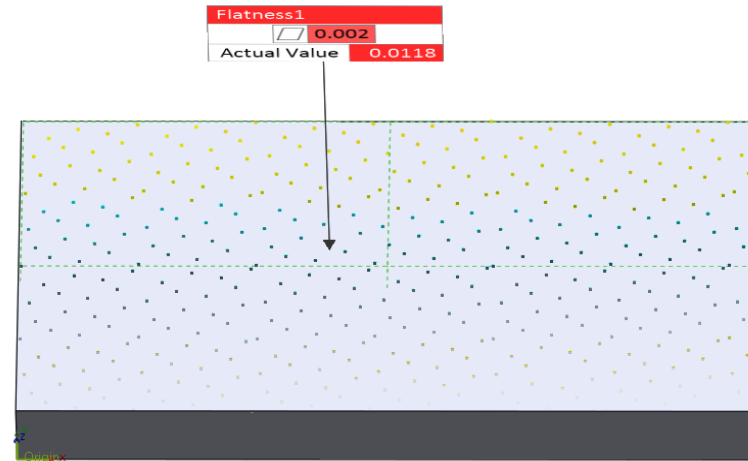
Figure 21. Sample #6 Flatness Deviation Measured Data vs. CAD Finish Pass

5.2 Measured Data Comparison

The data measured by both the measuring instruments are compared to find the difference between them and consequently, to find how deviated they are from each other. The data used for the comparison through the scan collection of each of the six samples using ScanArm®, and the average gap distance between the cloud of points of the scan and the sampling data from CMM is shown in Figure 22 where actual sampling are the points obtained from the sampling strategy, scanned data are the points which are closer in the cloud of points to the sampling points and gap vector which is the distance between each component. There is also a component called gap distance that corresponds to a scalar calculating the distance from one point to another

No.	Reference Pos. X	Reference Pos. Y	Reference Pos. Z	Measured Pos. X	Measured Pos. Y	Measured Pos. Z	Gap Vec. X	Gap Vec. Y	Gap Vec. Z	Gap Dist.
0	0.01	0.9941	0.7307	-0.0024	0.9953	0.7352	-0.0124	0.0012	0.0045	0.0132
1	0.0125	2.4964	0.7276	0.0089	2.4955	0.7344	-0.0036	-0.0009	0.0068	0.0078
2	0.0203	0.2461	0.7366	0.0203	0.2461	0.7375	0	0	0.0009	0.0009
3	0.0318	1.7455	0.7337	0.0318	1.7455	0.7353	0	0	0.0016	0.0016
.										.
.										.
.										.
509	5.7643	2.7476	0.7323	5.7642	2.7473	0.7354	-0.0001	-0.0003	0.0031	0.0031
510	5.7752	0.4979	0.7356	5.7752	0.4979	0.7386	0	0	0.003	0.003
511	5.7868	1.9973	0.7331	5.7868	1.9973	0.7363	0	0	0.0032	0.0032

Figure 22. Comparison calculations for measured data

5.2.1 Comparison for Rough Pass

In *Table 5* it is displayed the difference between each sampling method and scan data. APPENDIX C shows the average gap for component Z for flatness that helps to see how far the data obtained with CMM and AACMM is from the perfect form for the rough pass. (target is 0.73 in) and APPENDIX D shows the average gap for component Z for flatness that helps to see how far the data obtained with CMM and AACMM is from the perfect form for rough pass (the target 0.67 in).

37

| Avg. Gap Distance (in) from scan data to sample data				
		CMM measured data		
	SAMPLE	Aligned Systematic	Halton-Zaremba	Hammersley
AACMM data	S1	0.0019	0.0017	0.0024
	S2	0.0028	0.0027	0.0024
	S3	0.0015	0.0014	0.0012
	S4	0.0017	0.0021	0.0021
	S5	0.0021	0.0004	0.0007
	S6	0.0015	0.0015	0.0014

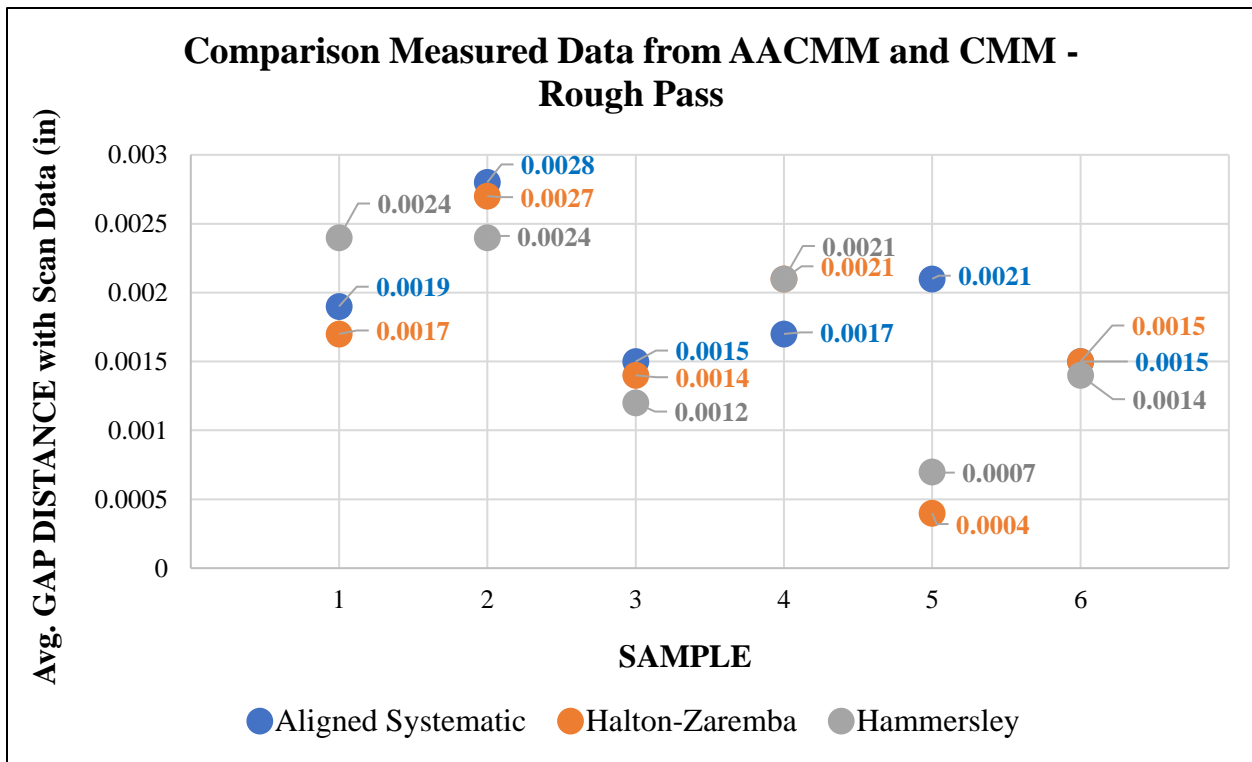*Table 5. Comparison Between Measured Data from CMM & AACMM – Rough Pass*

Figure 23 Comparison Between Measured Data Collected with AACMM & CMM

Color map shows in green the fitting points of the sampling strategies and scanned data. In red and shades of orange the points that overpass the tolerance zone and in blue and shades of blue the points that are under the tolerance zone. *Figure 24* for sample#1 shows the three sampling strategies compared with the scanning data. For Aligned Systematic and Halton Zaremba there is an area that fits but it presents almost half of the surface in orange, which indicates there is a difference over the tolerance zone for the sample points. Hammersley's sample shows a small fit

middle zone and a bad fitting in the sides. The distribution of points is skewed for aligned systematic and Halton-Zaremba.

Figure 25 shows the distribution of gap distances between measured data and scan data as shown in *Table 6*.

	S1					
	AS		H-Z		H	
	6 Sigma		6 Sigma		6 Sigma	
	# Points	%	# Points	%	# Points	%
-6σ	0	0.00%	1	0.195%	0	0.00%
-5σ	0	0.00%	0	0.000%	0	0.00%
-4σ	0	0.00%	1	0.195%	0	0.00%
-3σ	1	0.25%	12	2.344%	3	0.75%
-2σ	31	7.75%	62	12.109%	76	19.00%
-1σ	151	37.75%	168	32.813%	125	31.25%
1σ	178	44.50%	188	36.719%	116	29.00%
2σ	28	7.00%	67	13.086%	77	19.25%
3σ	3	0.75%	8	1.563%	2	0.50%
4σ	1	0.25%	0	0.000%	0	0.00%
5σ	1	0.25%	0	0.000%	0	0.00%
6σ	0	0.00%	1	0.195%	0	0.00%

Table 6. Sample #1 Rough pass points distribution

Figure 26 shows the distribution of gap distances between measured data and scan data as shown in *Table 7*.

	S2					
	AS		H-Z		H	
	6 Sigma		6 Sigma		6 Sigma	
	# Points	%	# Points	%	# Points	%
-6σ	0	0.00%	0	0.000%	0	0.00%
-5σ	0	0.00%	0	0.000%	0	0.00%
-4σ	2	0.50%	1	1.195%	2	0.50%
-3σ	13	3.25%	6	1.172%	6	1.50%
-2σ	50	12.50%	49	9.570%	41	10.25%
-1σ	125	31.25%	188	36.719%	146	36.50%
1σ	147	36.75%	228	44.531%	159	39.75%
2σ	59	14.75%	31	6.055%	39	9.75%
3σ	4	1.00%	0	0.000%	0	0.00%
4σ	0	0.00%	0	0.000%	1	0.25%
5σ	0	0.00%	1	0.195%	0	0.00%
6σ	0	0.00%	1	0.195%	0	0.00%

Table 7. Sample #2 Rough pass points distribution

Figure 27 shows the distribution of gap distances between measured data and scan data as shown in *Table 8*.

	S3					
	AS		H-Z		H	
	6 Sigma		6 Sigma		6 Sigma	
	# Points	%	# Points	%	# Points	%
-6σ	0	0.0000%	0	0.0000%	0	0.0000%
-5σ	0	0.0000%	0	0.0000%	0	0.0000%
-4σ	0	0.0000%	1	0.1957%	0	0.0000%
-3σ	8	2.0000%	6	1.1742%	5	1.2531%
-2σ	59	14.7500%	68	13.3072%	68	17.0426%
-1σ	128	32.0000%	165	32.2896%	123	30.8271%
1σ	130	32.5000%	186	36.3992%	139	34.8371%
2σ	60	15.0000%	74	14.4814%	58	14.5363%
3σ	5	1.2500%	6	1.1742%	1	0.2506%
4σ	0	0.0000%	0	0.0000%	1	0.2506%
5σ	0	0.0000%	0	0.0000%	1	0.2506%
6σ	0	0.0000%	0	0.0000%	0	0.0000%

Table 8. Sample #3 Rough pass points distribution

Figure 28 shows the distribution of gap distances between measured data and scan data as shown in *Table 9*.

	S4					
	AS		H-Z		H	
	6 Sigma		6 Sigma		6 Sigma	
	# Points	%	# Points	%	# Points	%
-6σ	0	0.0000%	0	0.0000%	0	0.0000%
-5σ	0	0.0000%	0	0.0000%	0	0.0000%
-4σ	0	0.0000%	0	0.0000%	0	0.0000%
-3σ	1	0.2500%	0	0.0000%	0	0.0000%
-2σ	35	8.7500%	0	0.0000%	0	0.0000%
-1σ	187	46.7500%	337	65.8203%	304	76.0000%
1σ	142	35.5000%	146	28.5156%	77	19.2500%
2σ	7	1.7500%	8	1.5625%	2	0.5000%
3σ	7	1.7500%	2	0.3906%	1	0.2500%
4σ	5	1.2500%	2	0.3906%	2	0.5000%
5σ	5	1.2500%	3	0.5859%	2	0.5000%
6σ	1	0.2500%	0	0.0000%	3	0.7500%

Table 9. Sample #4 Rough pass points distribution

Figure 29 shows the distribution of gap distances between measured data and scan data as shown in *Table 10*.

	S5					
	AS		H-Z		H	
	6 Sigma		6 Sigma		6 Sigma	
	# Points	%	# Points	%	# Points	%
-6σ	0	0.0000%	0	0.0000%	1	0.2500%
-5σ	0	0.0000%	3	0.5859%	0	0.0000%
-4σ	1	0.2500%	1	0.1953%	0	0.0000%
-3σ	2	0.5000%	2	0.3906%	2	0.5000%
-2σ	44	11.0000%	5	0.9766%	4	1.0000%
-1σ	154	38.5000%	269	52.5391%	205	51.2500%
1σ	158	39.5000%	177	34.5703%	160	40.0000%
2σ	19	4.7500%	26	5.0781%	12	3.0000%
3σ	2	0.5000%	19	3.7109%	8	2.0000%
4σ	7	1.7500%	0	0.0000%	0	0.0000%
5σ	1	0.2500%	1	0.1953%	1	0.2500%
6σ	2	0.5000%	0	0.0000%	0	0.0000%

Table 10. Sample #5 Rough pass points distribution

Figure 29 shows the distribution of gap distances between measured data and scan data as shown in *Table 11*.

|	S6					
	AS		H-Z		H	
	6 Sigma		6 Sigma		6 Sigma	
	# Points	%	# Points	%	# Points	%
-6σ	0	0.0000%	0	0.0000%	0	0.0000%
-5σ	0	0.0000%	1	0.1953%	1	0.2500%
-4σ	0	0.0000%	0	0.0000%	1	0.2500%
-3σ	9	2.2500%	0	0.0000%	0	0.0000%
-2σ	51	12.7500%	11	2.1484%	1	0.2500%
-1σ	134	33.5000%	252	49.2188%	200	50.0000%
1σ	135	33.7500%	230	44.9219%	182	45.5000%
2σ	50	12.5000%	2	0.3906%	2	0.5000%
3σ	10	2.5000%	1	0.1953%	1	0.2500%
4σ	1	0.2500%	1	0.1953%	0	0.0000%
5σ	0	0.0000%	0	0.0000%	2	0.5000%
6σ	0	0.0000%	1	0.1953%	0	0.0000%

Table 11. Sample #6 Rough pass points distribution

SAMPLE#1 STEEL 1018
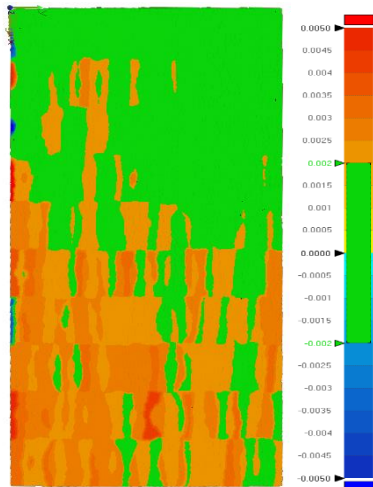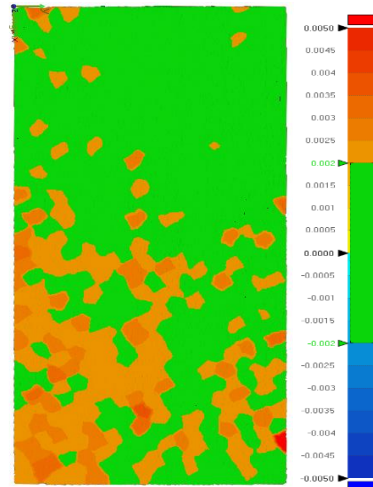
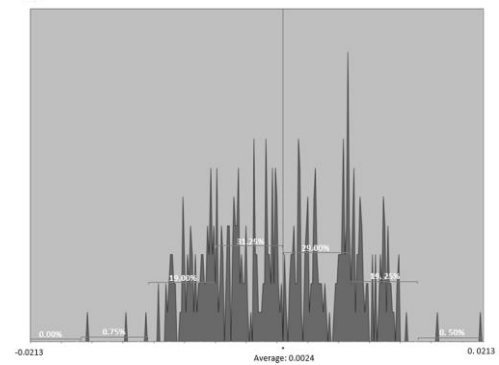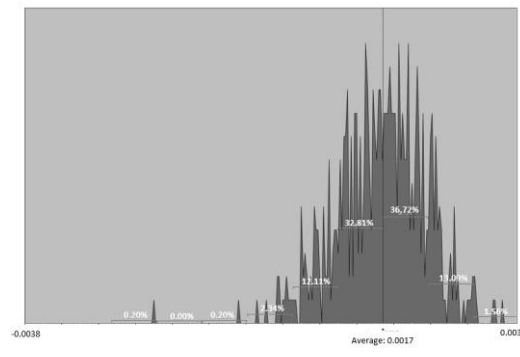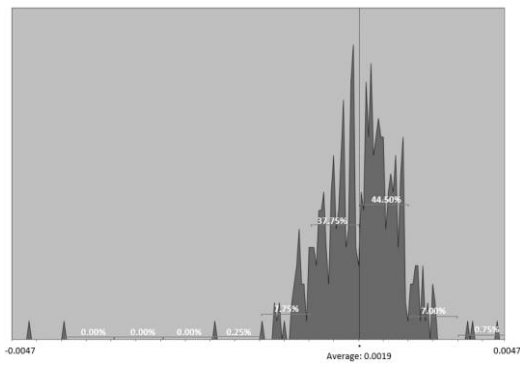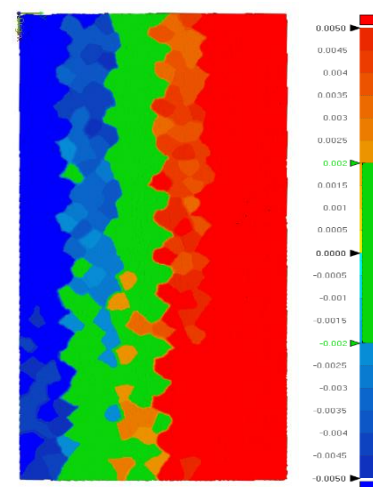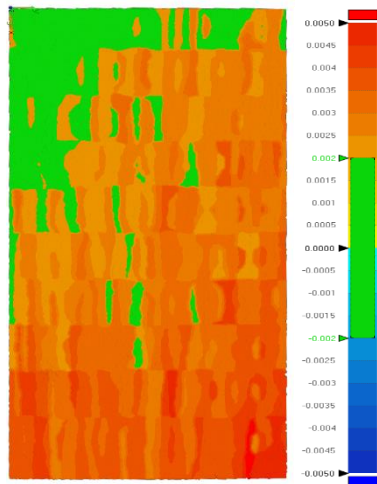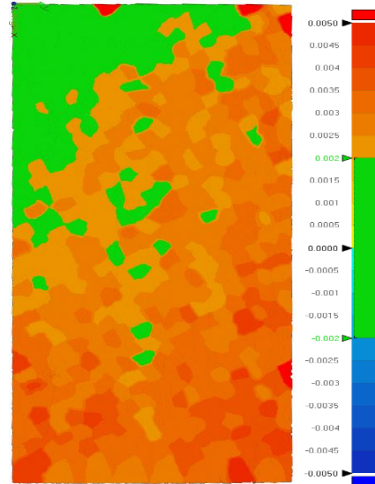| ALIGNED SYSTEMATIC | HALTON-ZAREMBA | HAMMERSLEY |

Figure 24 Sampling Data Compared with Scanned Data for Sample#1 – Rough pass

SAMPLE#2 STEEL 1018

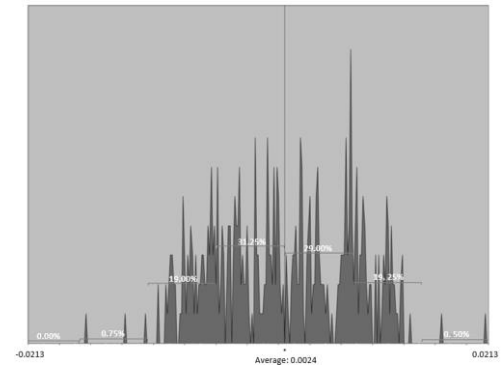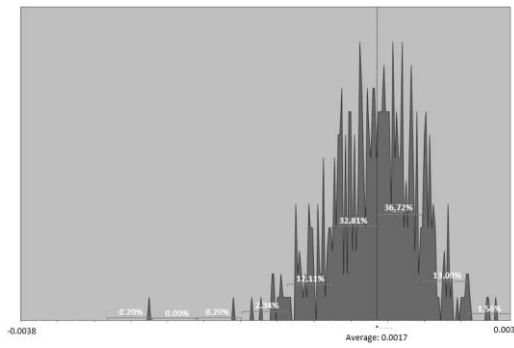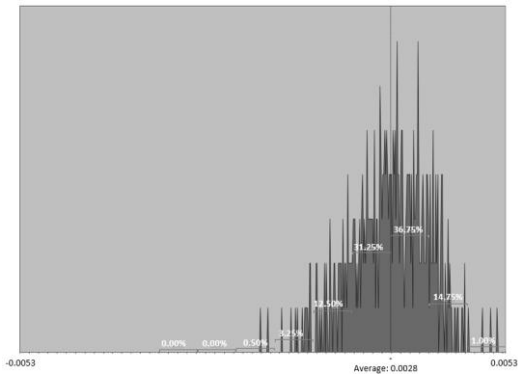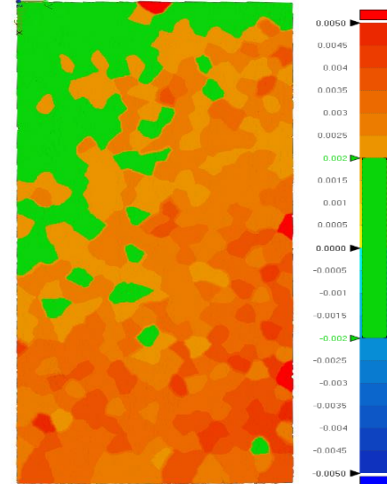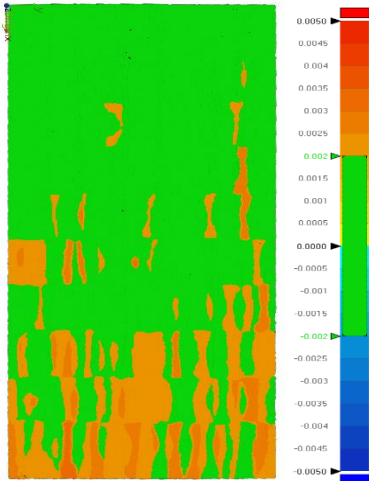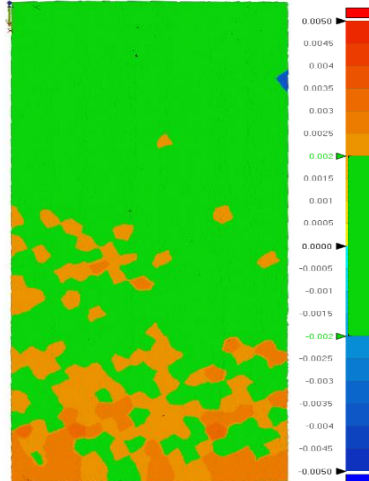**ALIGNED SYSTEMATIC** **HALTON-ZAREMBA** **HAMMERSLEY**

Figure 25. Sampling Data Compared with Scanned Data for Sample#2 – Rough pass

SAMPLE#3 STEEL 1018

ALIGNED SYSTEMATIC

HALTON-ZAREMBA
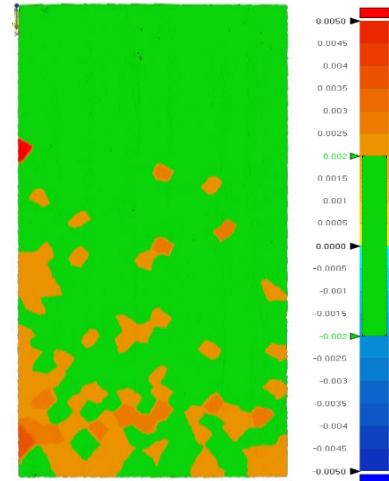
HAMMERSLEY

Figure 26. Sampling Data Compared with Scanned Data for Sample#3 – Rough pass

SAMPLE#4 ALUMINUM 6061
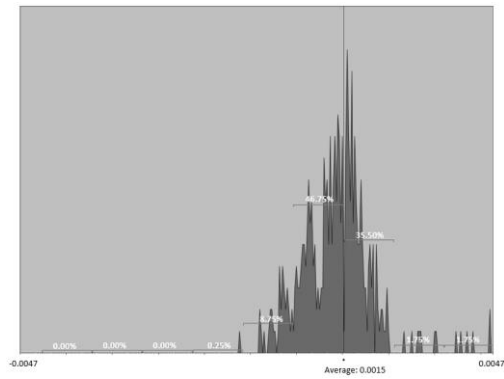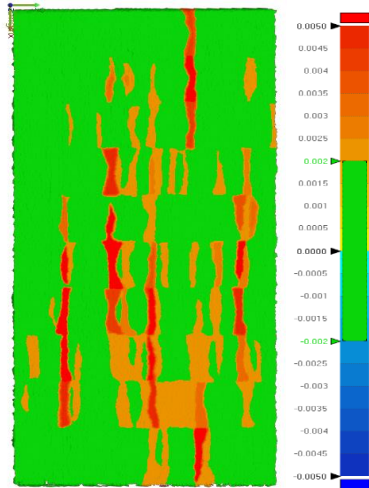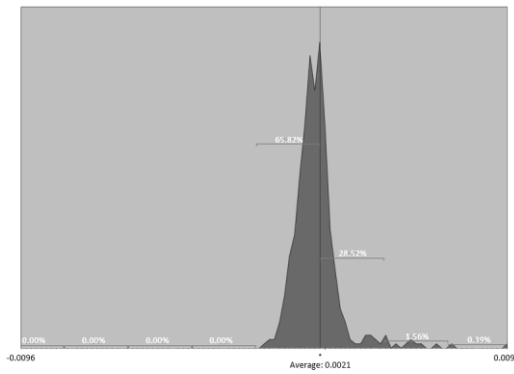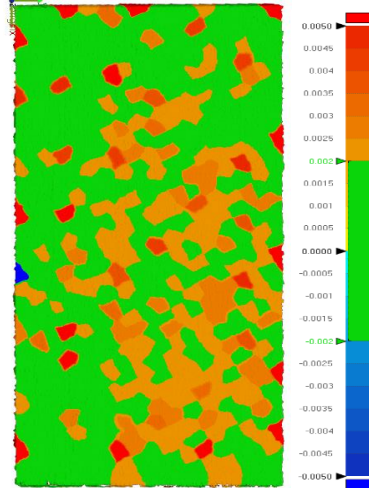
ALIGNED SYSTEMATIC   HALTON-ZAREMBA   HAMMERSLEY
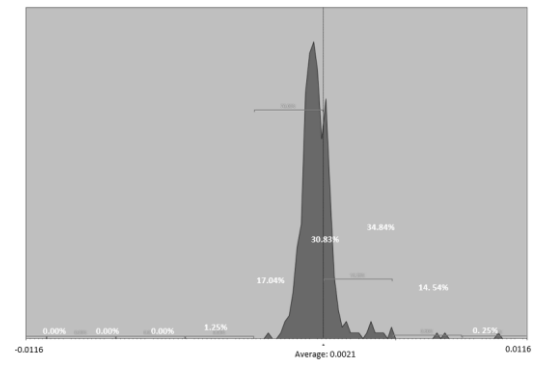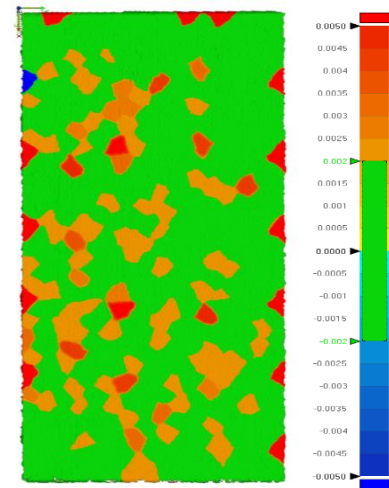
Figure 27. Sampling Data Compared with Scanned Data for Sample#4 – Rough pass

SAMPLE#5 ALUMINUM 6061
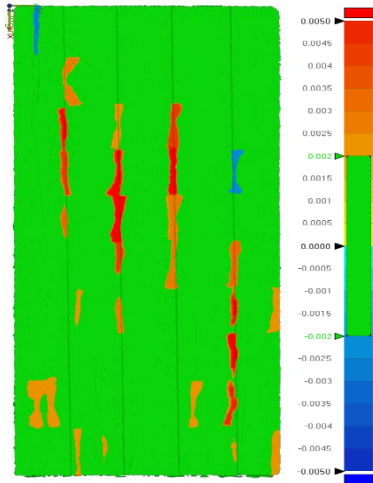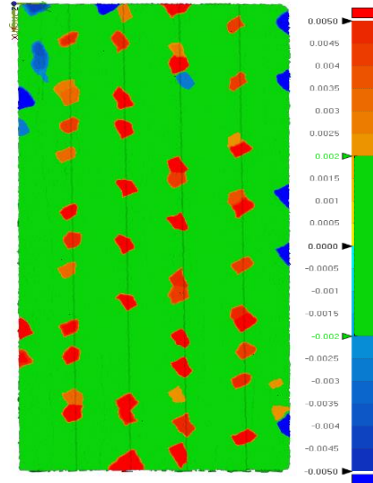
| ALIGNED SYSTEMATIC | HALTON-ZAREMBA | HAMMERSLEY |
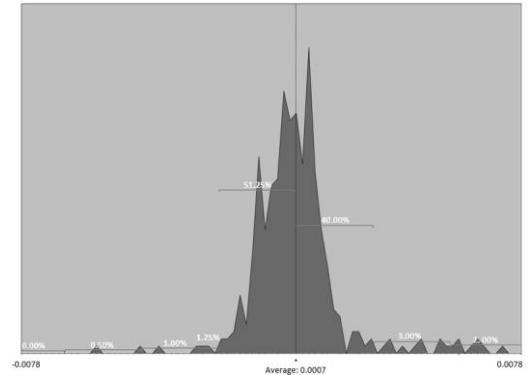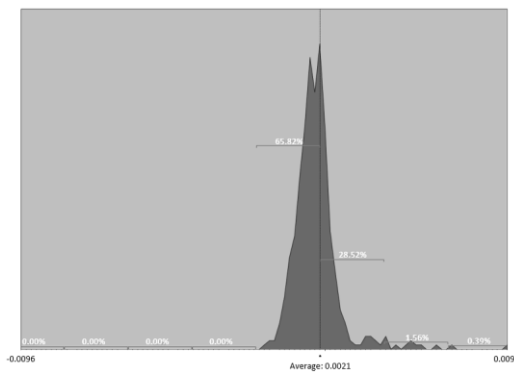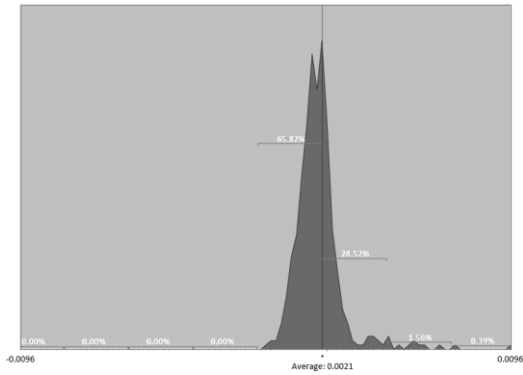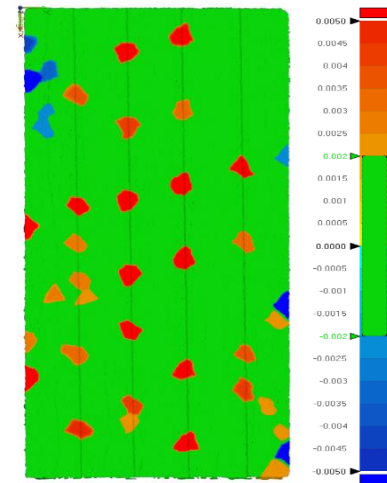
Figure 28. Sampling Data Compared with Scanned Data for Sample#5 – Rough pass

SAMPLE#6 ALUMINUM 6061
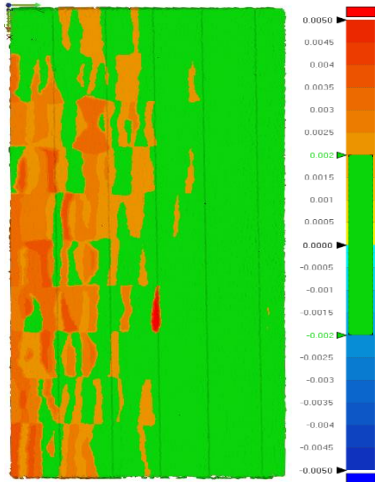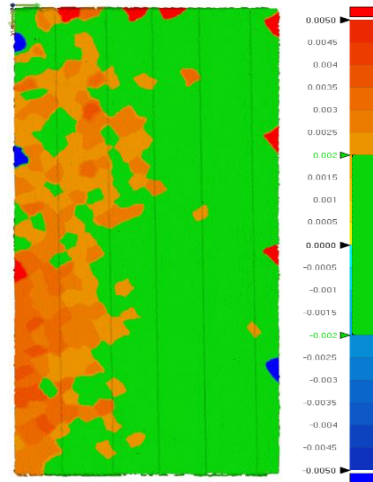
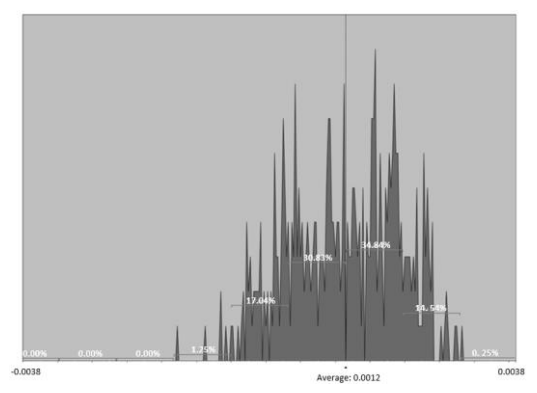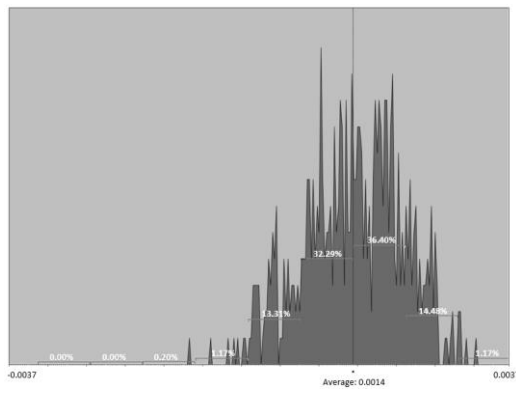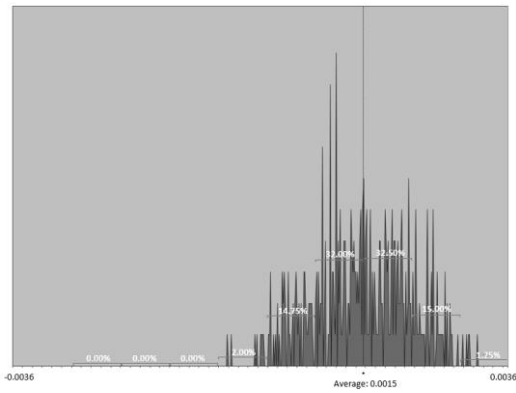| ALIGNED SYSTEMATIC	HALTON-ZAREMBA	HAMMERSLEY
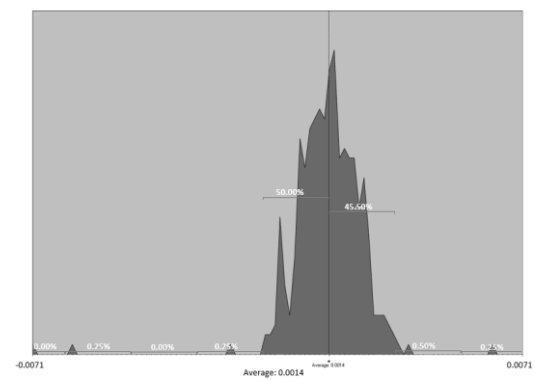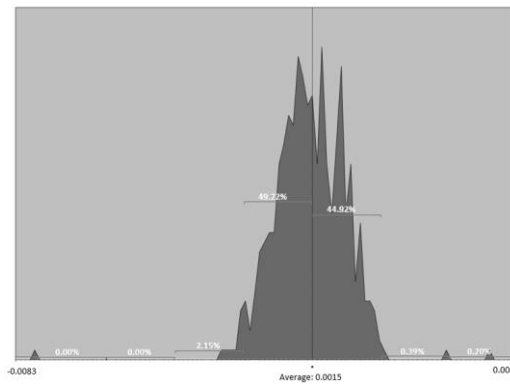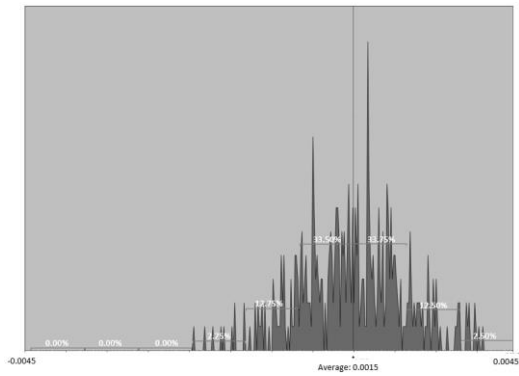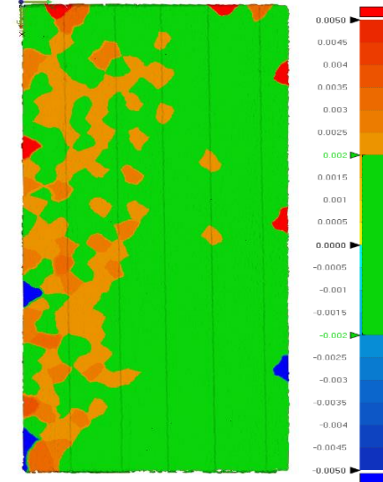
Figure 29. Sampling Data Compared with Scanned Data for Sample#6 – Rough pass

5.2.2 Comparison for Finish Pass

| | | Std. Dev = Avg. Gap Dist (in) | | |
| | | CMM data | | |
	SAMPLE	Aligned Systematic	Halton-Zaremba	Hammersley
AACMM	S1	0.002	0.0018	0.0019
	S2	0.0012	0.00086	0.00099
	S3	-0.00019	-0.00085	-0.0014
	S4	0.00056	0.0019	0.0027
	S5	0.0023	0.0025	0.0023
	S6	-0.0071	-0.0069	-0.0065

Table 12. Comparison Between Measured Data from CMM & AACMM – Finish Pass
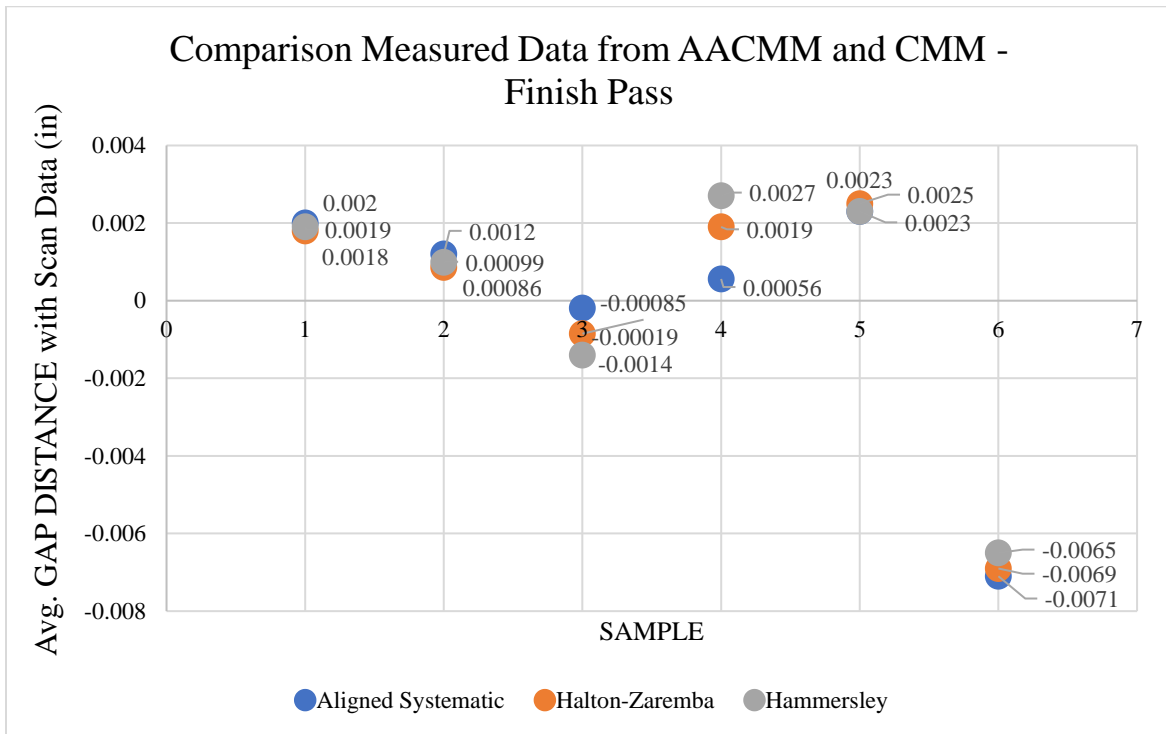
Figure 30. 3D Comparison Measured Data

*Figure 31*Figure 25 shows the distribution of gap distances between measured data and scan data as shown in *Table 13* .

	S1					
	AS		H-Z		H	
	6 Sigma		6 Sigma		6 Sigma	
-6σ	0	0.00%	0	0.000%	0	0.00%
-5σ	0	0.00%	1	0.195%	0	0.00%
-4σ	1	0.25%	1	0.195%	1	0.25%
-3σ	7	1.75%	8	1.563%	7	1.75%
-2σ	42	10.50%	70	13.672%	48	12.03%
-1σ	162	40.50%	175	34.180%	148	37.09%
1σ	139	34.75%	173	33.789%	135	33.83%
2σ	37	9.25%	69	13.477%	49	12.28%
3σ	4	1.00%	9	1.758%	8	2.01%
4σ	0	0.00%	2	0.391%	2	0.50%
5σ	1	0.25%	0	0.000%	1	0.25%
6σ	1	0.25%	0	0.000%	0	0.00%

Table 13. Sample #1 Finish pass points distribution

Figure 32 shows the distribution of gap distances between measured data and scan data as shown in *Table 14* .

	S2					
	AS		H-Z		H	
	6 Sigma		6 Sigma		6 Sigma	
-6σ	0	0.00%	0	0.000%	0	0.00%
-5σ	0	0.00%	0	0.000%	0	0.00%
-4σ	0	0.00%	0	0.000%	0	0.00%
-3σ	1	0.25%	7	1.367%	6	1.50%
-2σ	49	12.25%	61	11.914%	58	14.50%
-1σ	163	40.75%	203	39.648%	136	34.00%
1σ	141	35.25%	147	28.711%	128	32.00%
2σ	35	8.75%	80	15.625%	59	14.75%
3σ	3	0.75%	10	1.953%	9	2.25%
4σ	1	0.25%	0	0.000%	1	0.25%
5σ	2	0.50%	1	0.195%	0	0.00%
6σ	2	0.50%	1	0.195%	0	0.00%

Table 14. Sample #2 Finish pass points distribution

Figure 33 shows the distribution of gap distances between measured data and scan data as shown in *Table 15*.

	S3					
	AS		H-Z		H	
	6 Sigma		6 Sigma		6 Sigma	
-6σ	1	0.25%	0	0.000%	0	0.00%
-5σ	0	0.00%	0	0.000%	1	0.25%
-4σ	0	0.00%	2	0.391%	1	0.25%
-3σ	1	0.25%	6	1.172%	10	2.50%
-2σ	24	6.00%	50	9.766%	42	10.50%
-1σ	187	46.75%	199	38.867%	135	33.75%
1σ	158	39.50%	208	40.625%	144	36.00%
2σ	18	4.50%	35	6.836%	57	14.25%
3σ	2	0.50%	4	0.781%	4	1.00%
4σ	0	0.00%	0	0.000%	2	0.50%
5σ	0	0.00%	0	0.000%	0	0.00%
6σ	0	0.00%	1	0.195%	0	0.00%

Table 15. Sample #3 Finish pass points distribution

Figure 34 shows the distribution of gap distances between measured data and scan data as shown in *Table 16*.

	S4					
	AS		H-Z		H	
	6 Sigma		6 Sigma		6 Sigma	
-6σ	0	0.00%	0	0.000%	0	0.00%
-5σ	0	0.00%	0	0.000%	1	0.25%
-4σ	0	0.00%	2	0.391%	0	0.00%
-3σ	3	0.75%	8	1.563%	7	1.75%
-2σ	37	9.25%	62	12.109%	47	11.75%
-1σ	173	43.25%	184	35.938%	149	37.25%
1σ	146	36.50%	189	36.914%	135	33.75%
2σ	29	7.25%	51	9.961%	44	11.00%
3σ	2	0.50%	10	1.953%	11	2.75%
4σ	0	0.00%	1	0.195%	0	0.00%
5σ	0	0.00%	0	0.000%	1	0.25%
6σ	0	0.00%	0	0.000%	0	0.00%

Table 16. Sample #4 Finish pass points distribution

Figure 35 shows the distribution of gap distances between measured data and scan data as shown in *Table 17*.

	S5					
	AS		H-Z		H	
	6 Sigma		6 Sigma		6 Sigma	
-6σ	0	0.00%	0	0.000%	0	0.00%
-5σ	0	0.00%	0	0.000%	1	0.25%
-4σ	0	0.00%	1	0.195%	1	0.25%
-3σ	4	1.00%	11	2.148%	6	1.50%
-2σ	65	16.25%	78	15.234%	50	12.50%
-1σ	139	34.75%	148	28.906%	128	32.00%
1σ	117	29.25%	200	39.063%	169	42.25%
2σ	73	18.25%	63	12.305%	40	10.00%
3σ	1	0.25%	6	1.172%	3	0.75%
4σ	1	0.25%	0	0.000%	0	0.00%
5σ	0	0.00%	2	0.391%	0	0.00%
6σ	0	0.00%	0	0.000%	0	0.00%

Table 17. Sample #5 Finish pass points distribution

Figure 36 shows the distribution of gap distances between measured data and scan data as shown in *Table 18.*

	S6					
	AS		H-Z		H	
	6 Sigma		6 Sigma		6 Sigma	
-6σ	0	0.00%	0	0.000%	0	0.00%
-5σ	0	0.00%	0	0.000%	0	0.00%
-4σ	0	0.00%	0	0.000%	1	0.25%
-3σ	0	0.00%	2	0.391%	0	0.00%
-2σ	69	17.25%	91	17.773%	74	18.50%
-1σ	132	33.00%	163	31.836%	129	32.25%
1σ	114	28.50%	152	29.688%	111	27.75%
2σ	85	21.25%	103	20.117%	84	21.00%
3σ	0	0.00%	0	0.000%	0	0.00%
4σ	0	0.00%	0	0.000%	0	0.00%
5σ	0	0.00%	0	0.000%	0	0.00%
6σ	0	0.00%	0	0.000%	0	0.00%

Table 18. Sample #6 Finish pass points distribution

SAMPLE#1 STEEL 1018 – FINISH PASS
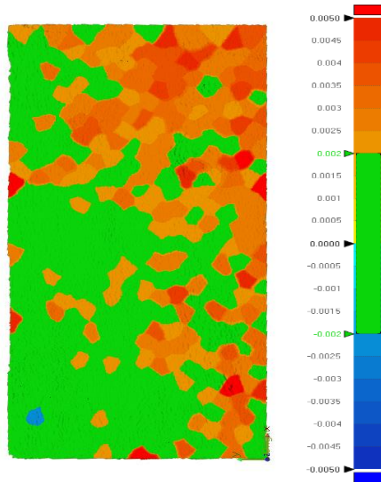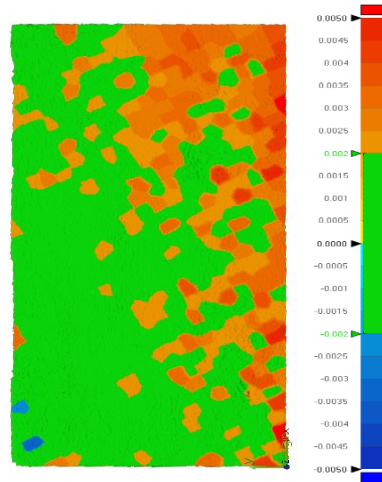
ALIGNED SYSTEMATIC	HALTON-ZAREMBA	HAMMERSLEY
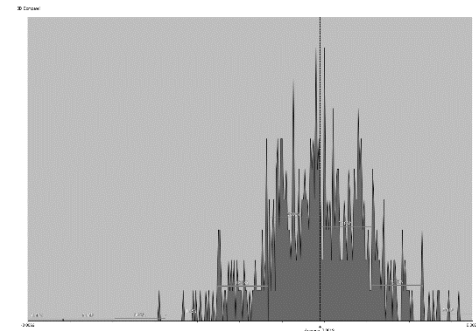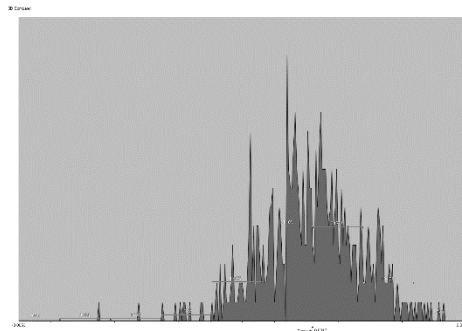
Figure 31. Sampling Data Compared with Scanned Data for Sample#1 – Finish pass

SAMPLE#2 STEEL 1018 – FINISH PASS

ALIGNED SYSTEMATIC   **HALTON-ZAREMBA**   **HAMMERSLEY**
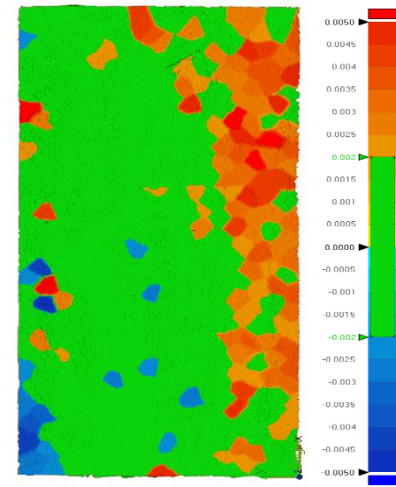
Figure 32. Sampling Data Compared with Scanned Data for Sample#2 – Finish pass

SAMPLE#3 STEEL 1018 – FINISH PASS
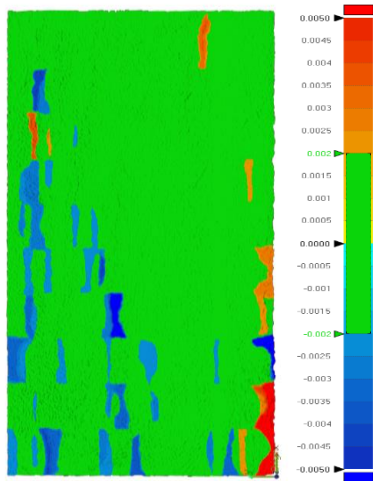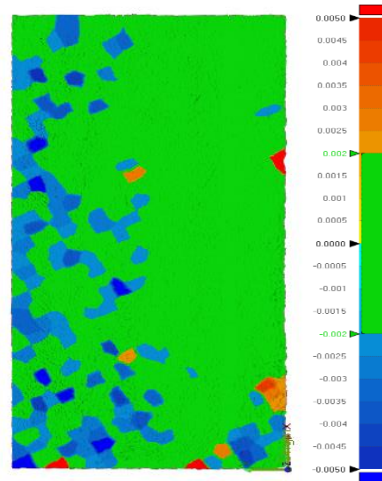
ALIGNED SYSTEMATIC   **HALTON-ZAREMBA**   **HAMMERSLEY**
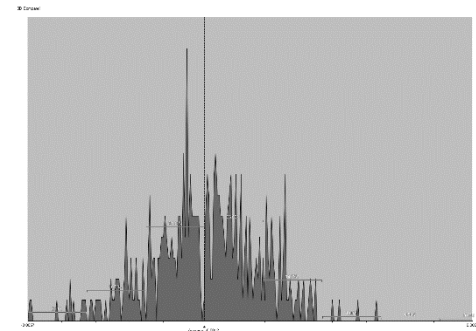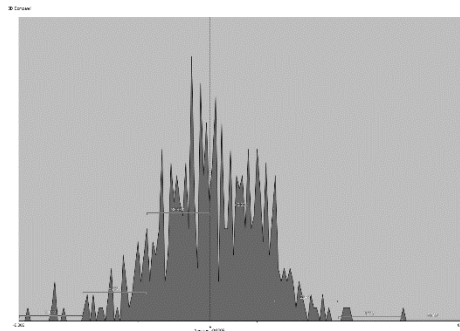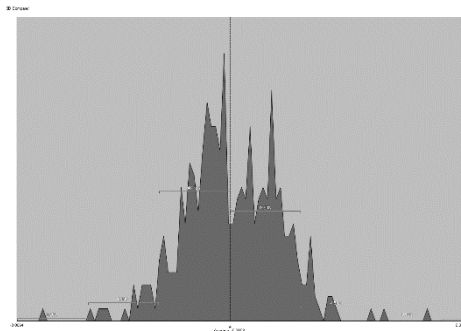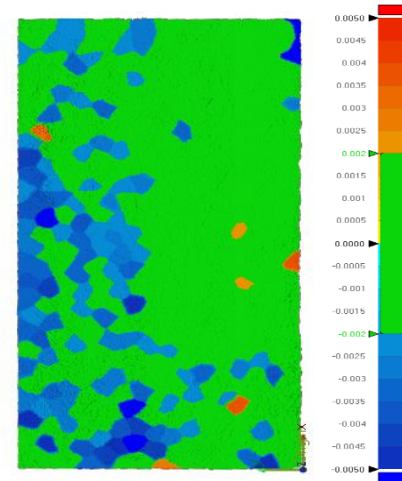
Figure 33. Sampling Data Compared with Scanned Data for Sample#3 – Finish pass

SAMPLE#4 ALUMINUM 6061 – FINISH PASS
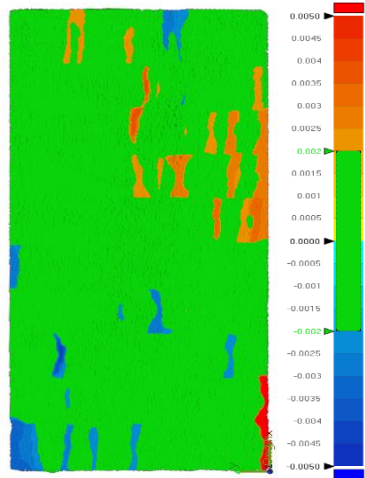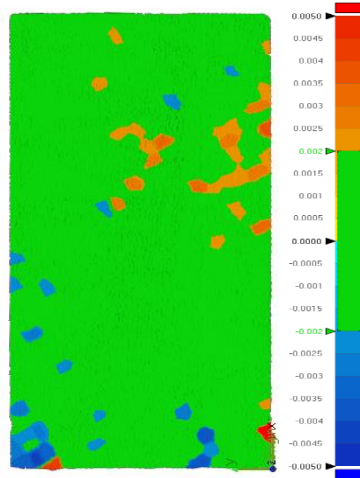
ALIGNED SYSTEMATIC	HALTON-ZAREMBA	HAMMERSLEY
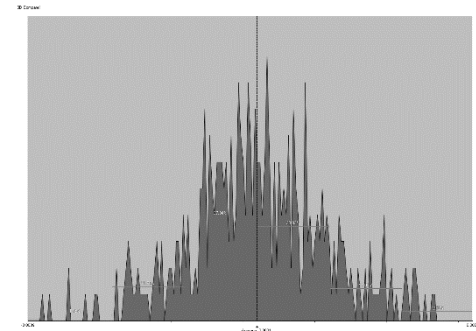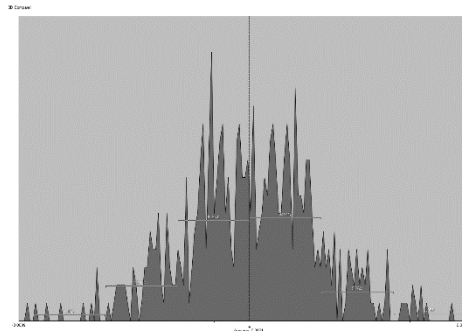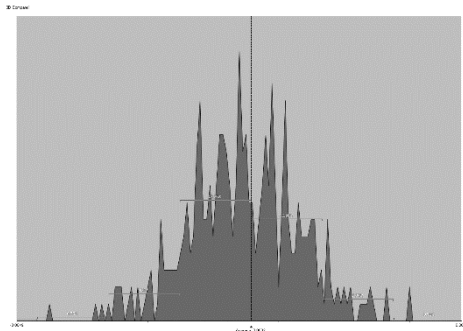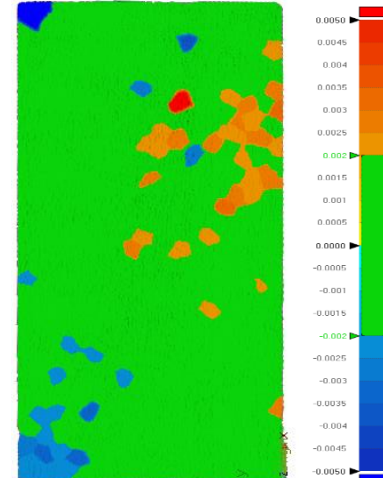
Figure 34. Sampling Data Compared with Scanned Data for Sample#4 – Finish pass

SAMPLE#5 ALUMINUM 6061 – FINISH PASS
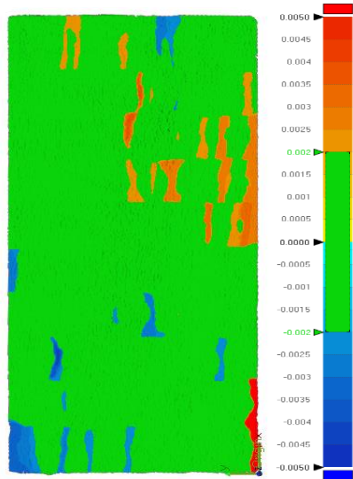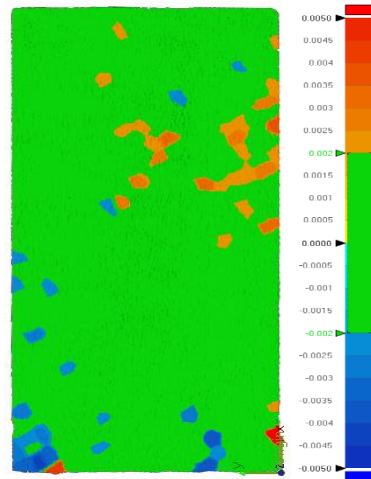
ALIGNED SYSTEMATIC   **HALTON-ZAREMBA**   **HAMMERSLEY**
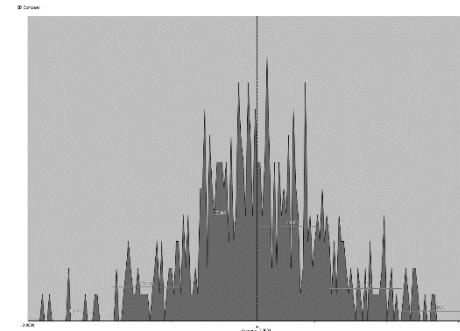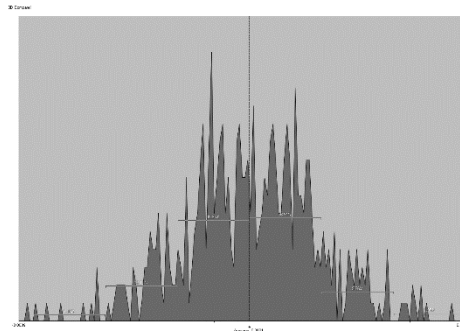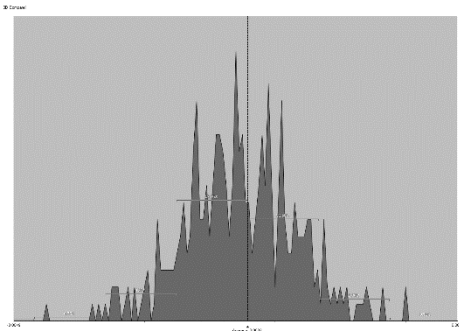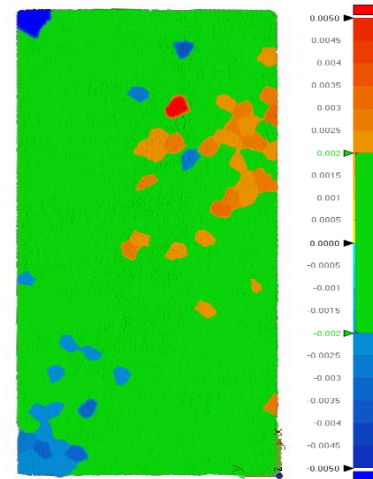
Figure 35. Sampling Data Compared with Scanned Data for Sample#5 – Finish pass

SAMPLE#6 ALUMINUM 6061 – FINISH PASS
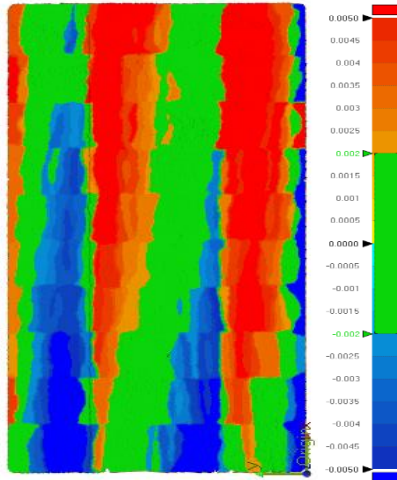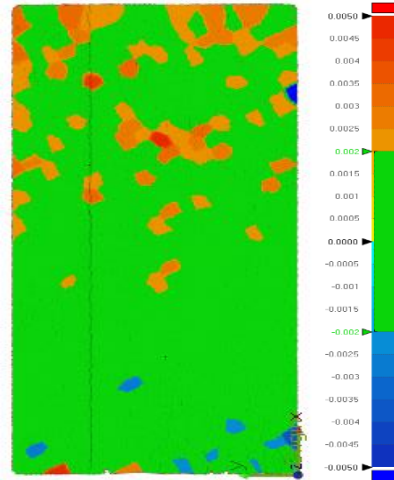
ALIGNED SYSTEMATIC   **HALTON-ZAREMBA**   **HAMMERSLEY**

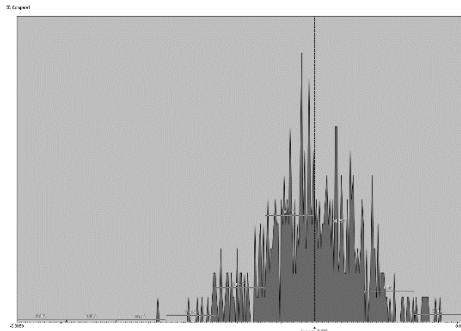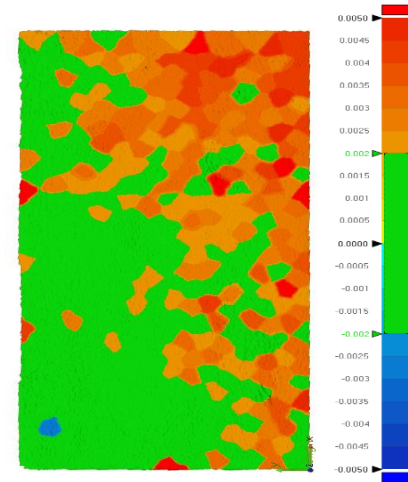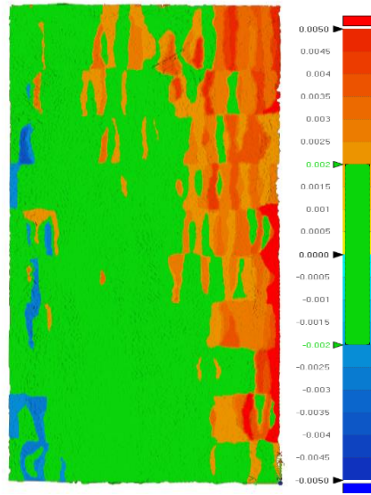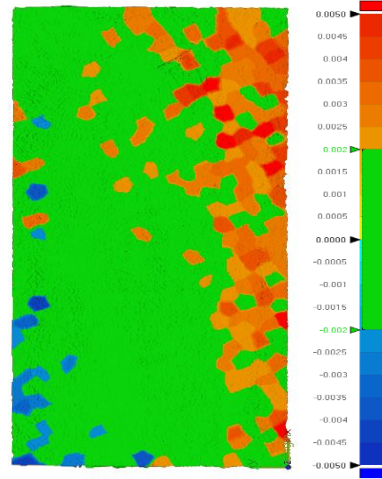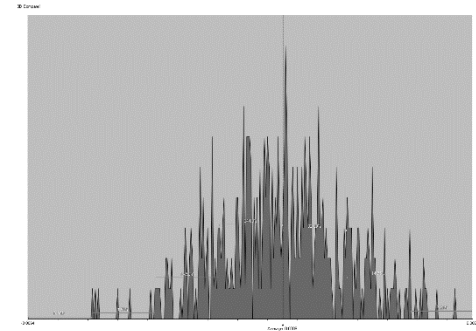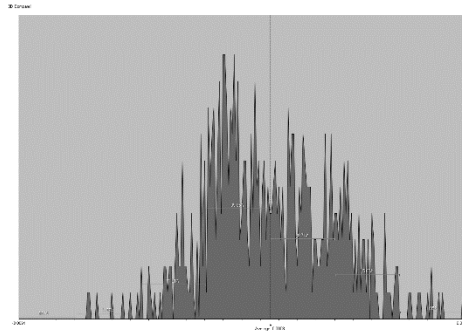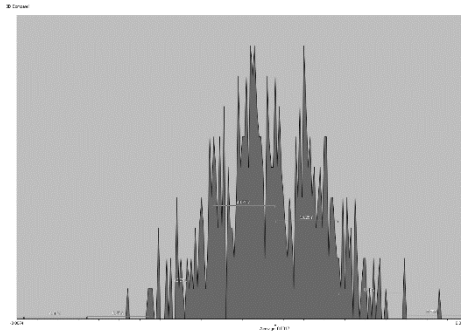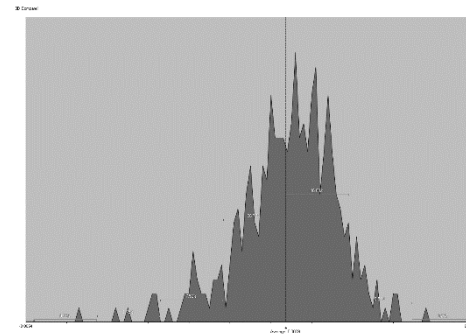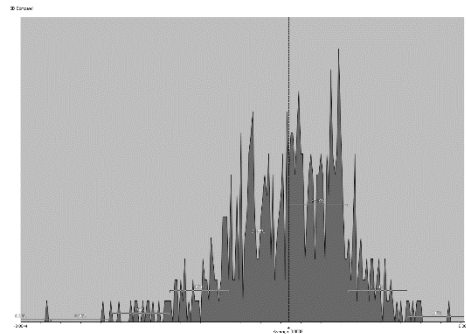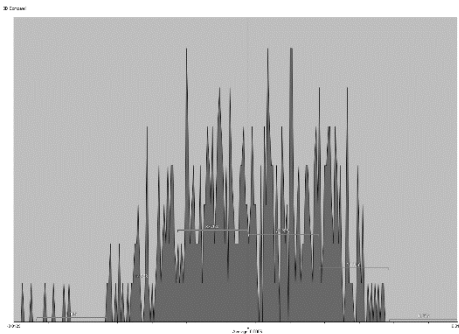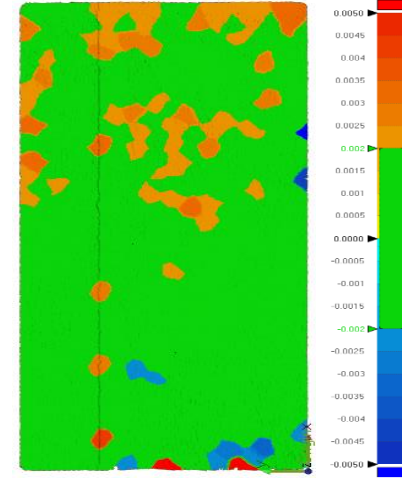*Figure 36. Sampling Data Compared with Scanned Data for Sample#6 – Finish pass*

5.3 CONCLUSIONS

Results obtained from the verification of flatness after a rough pass operation are shown in *Table 3* and *Figure 18*. These show that results obtained with CMM are more precise than the ones obtained with AACMM. The differences are not considered large, but still significant. From these measurements, it is observed that Aligned Systematic strategy is not sufficient to describe flatness, possibly due to the big gap between one row to another. Thus manufacturing patterns would have a big role that could miss important information. Similarly, in *Table 4* and *Figure 19* the behavior of the data supports the conclusion that both inspections taken with AACMM and CMM data represent flatness deviation well enough and are comparable.

This means that it is possible to inspect a part using AACMM with relatively good precision and consuming less time than the CMM, given that there is no need for surveying the surface using sampling methods and creating algorithms to obtain points and calculate the error.

For a comparison between the measured data, via *Table 5* and *Figure 23,* we continue seeing that the results are close, and it is important to highlight that a careful alignment and origin definition for data obtained using both measuring instruments is critical to compare the results.

It is also important to mention that Aluminum 6061 is a more ductile material than Steel 6061, causing problems to the finishing of the part. It creates surface texture and imperfections in the surface making it more difficult to inspect with the laser scanner.

More investigation of other geometries must be undertaken before formal conclusions can be reached regarding the feasibility of using AACMMs as commercial alternatives to CMMs in part verification in industry.

REFERENCES

Acero, R., Brau, A., Santolaria, J., & Pueo, M. (2015). Verification of an articulated arm coordinate measuring machine using a laser tracker as reference equipment and an indexed metrology platform. *Measurement: Journal of the International Measurement Confederation*, *69*, 52–63. https://doi.org/10.1016/j.measurement.2015.03.023

Aguado, S., Santolaria, J., Samper, D., & Aguilar, J. J. (2013). Influence of measurement noise and laser arrangement on measurement uncertainty of laser tracker multilateration in machine tool volumetric verification. *Precision Engineering*, *37*(4), 929–943. https://doi.org/10.1016/j.precisioneng.2013.03.006

Aguirre Cruz, J. A. (2007). *Decision support system for form verification of manufactured parts*. Dissertation. Department of Industrial and Systems Engineering. The University of Oklahoma.

ASME. (2009). *Dimensioning and Tolerancing Handbook*. New York, N.Y.: ASME. Retrieved from https://www.asme.org/codes-standards/find-codes-standards/y14-5-dimensioning-tolerancing

Badar, M. A., Raman, S., & Pulat, P. S. (2003). Intelligent Search-Based Selection of Sample Points for Straightness and Flatness Estimation. *Journal of Manufacturing Science and Engineering*, *125*(2), 263–271. https://doi.org/10.1115/1.1556859

Badar, M. A., Raman, S., & Pulat, P. S. (2005). Experimental verification of manufacturing error pattern and its utilization in form tolerance sampling. *International Journal of Machine Tools and Manufacture*.

https://doi.org/10.1016/j.ijmachtools.2004.06.017

Badar, M. A., Raman, S., Pulat, P. S., & Shehab, R. L. (2005). Experimental Analysis of Search-Based Selection of Sample Points for Straightness and Flatness Estimation. *Journal of Manufacturing Science and Engineering*. https://doi.org/10.1115/1.1828051

Badar, M. A., & Singhal, A. (2006). *Comparison of sampling methods for flatness evaluation using CMM. MS Thesis*. Department of Industrial and Mechanical Technology. Indiana State University. Retrieved from http://www.scopus.com/inward/record.url?eid=2-s2.0-84858452518&partnerID=MN8TOARS

Choi, W., & Kurfess, T. R. (1999). Dimensional measurement data analysis, part 1:A Zone Fitting Algorithm. *Journal of Manufacturing Science and Engineering, Transactions of the ASME*, *121*(2), 246–250. https://doi.org/10.1115/1.2831212

Cochran, W. G. (1977). *Sampling Techniques* (Third Edit). New York - Chichester - Brisbane - Toronto - Singapore: John Wiley & Sons.

Collins, C. E., Fay, E. B., Aguirre-Cruz, J. A., & Raman, S. (2007). Alternate methods for sampling in coordinate metrology. *Proceedings of the Institution of Mechanical Engineers, Part B: Journal of Engineering Manufacture*, *221*(6), 1041–1052. https://doi.org/10.1243/09544054JEM734

Cuesta, E., Rico, J. C., Fernández, P., Blanco, D., & Valiño, G. (2009). Influence of roughness on surface scanning by means of a laser stripe system. *International Journal of Advanced Manufacturing Technology*, *43*(11–12), 1157–1166. https://doi.org/10.1007/s00170-008-1794-9

Faro Laser ScanArm® V3 (PDF). (2010). Retrieved April 8, 2019, from
https://faro.app.box.com/s/6l9spp0jymjwkqkpoa85e6mlomlfx6eg

FaroArm® Platinum (PDF). (2010). Retrieved April 6, 2019, from
https://knowledge.faro.com/Hardware/Legacy-
Hardware/Legacy_USB_FaroArm-
ScanArm/Technical_Specification_Sheet_for_the_Platinum-Titanium-
Advantage

Ge, M., Fontaine, J. F., Coquet, R., Juillion, P., Hennebelle, F., & Romdhani, F.
(2014). Methodology for the assessment of measuring uncertainties of
articulated arm coordinate measuring machines. *Measurement Science and
Technology*, *25*(12), 125008. https://doi.org/10.1088/0957-0233/25/12/125008

Gomez, J. A. (n.d.). Excel VBA Delete Row: Step-by-Step Guide and 12 Code
Examples to Delete Rows with Macros #5: Delete Multiple Selected Rows.
Retrieved June 17, 2018, from https://powerspreadsheets.com/excel-vba-
delete-row/

Gromczak, K., Ostrowska, K., Owczarek, D., & Sładek, J. (2015). Validation of
the Metrological Model of Coordinate Measuring Arm Using Multifeature
Check. *Advances in Science and Technology Research Journal*, *9*(28), 120–
124. https://doi.org/10.12913/22998624/60798

Jalid, A., Hariri, S., & Laghzale, N. E. (2015). Influence of sample size on flatness
estimation and uncertainty in three-dimensional measurement. *International
Journal of Metrology and Quality Engineering*, *6*(1), 102.
https://doi.org/10.1051/ijmqe/2015002

Kalpakjian, Serope - Schmid, S. R. (2014). *Manufacturing Engineering and*

Technology (Seventh Ed). Singapore, London, New York, Toronto, Sydney, Tokyo, Madrid, Mexico City, Munich, Paris, Cape Town, Hong Kong, Montreal: Pearson. https://doi.org/10.1017/CBO9781107415324.004

Kim, W. S., & Raman, S. (2000). On the selection of flatness measurement points in coordinate measuring machine inspection. *International Journal of Machine Tools and Manufacture*, *40*(3), 427–443. https://doi.org/10.1016/S0890-6955(99)00059-0

Lee, G. (1997). Sampling Strategy Design for Dimensional Measurement of Geometric Features Using Coordinate Measuring Machine. *International Journal of Machine Tools and Manufacture*, *37*(7), 917–934.

Li, X. H., Chen, B., & Qiu, Z. R. (2013). The calibration and error compensation techniques for an Articulated Arm CMM with two parallel rotational axes. *Measurement: Journal of the International Measurement Confederation*, *46*(1), 603–609. https://doi.org/10.1016/j.measurement.2012.08.020

Luo, Z., Liu, H., Li, D., & Tian, K. (2018). Analysis and compensation of equivalent diameter error of articulated arm coordinate measuring machine. *Measurement and Control (United Kingdom)*, *51*(1–2), 16–26. https://doi.org/10.1177/0020294018755324

Markov, B. N., & Sharamkov, A. B. (2014). The Use of the Results of Calibration of Faro Arm Coordinate-Measuring Machines for Use in Comparative Estimation of Their Precision Capabilities. *Measurement Techniques*, *57*(8), 870–874. https://doi.org/10.1007/s11018-014-0551-8

Montgomery, D. C., Rugner, G. C., & Faris Hubele, N. (2011). *Engineering Statistics* (Fifth Edition). United States of America: John Wiley & Sons, Inc.

Obeidat, S. M., & Raman, S. (2011). Process-guided coordinate sampling of end-milled flat plates. *International Journal of Advanced Manufacturing Technology*, *53*(9–12), 979–991. https://doi.org/10.1007/s00170-010-2885-y

Raghunandan, R., & Rao, P. V. (2007). Selection of an optimum sample size for flatness error estimation while using coordinate measuring machine. *International Journal of Machine Tools and Manufacture*, *47*(3–4), 477–482. https://doi.org/10.1016/j.ijmachtools.2006.06.008

Raghunandan, R., & Venkateswara Rao, P. (2008). Selection of sampling points for accurate evaluation of flatness error using coordinate measuring machine. *Journal of Materials Processing Technology*, *202*(1–3), 240–245. https://doi.org/10.1016/j.jmatprotec.2007.09.066

Robert, J., & Paulo, H. (2011). *Coordinate Measuring Machines and Systems, Second Edition* (Vol. 20114347). https://doi.org/10.1201/b11022

Santolaria, J., Aguilar, J. J., Guillomía, D., & Cajal, C. (2011). A crenellated-target-based calibration method for laser triangulation sensors integration in articulated measurement arms. *Robotics and Computer-Integrated Manufacturing*, *27*(2), 282–291. https://doi.org/10.1016/j.rcim.2010.07.008

Systems, 3D. (2018). *Geomagic Control X^{TM}*. 3D Systems.

Technical specifications: Styli and accessories (pdf). (2016). Retrieved October 20, 2019, from https://www.renishaw.com/en/styli-for-faro-arms--43707

Webinars | 3D Systems. (2019). Retrieved April 10, 2019, from https://www.3dsystems.com/webinars?field_applications_target_id=246&field _industries_target_id=All

Woo, T. C., Liang, R., Hsieh, C. C., & Lee, N. K. (1995). Efficient sampling for surface measurements. *Journal of Manufacturing Systems*, *14*(5), 345–354. https://doi.org/10.1016/0278-6125(95)98871-3

APPENDICES

APPENDIX A: Python™ coding to calculate Sampling points snapshots

Aligned Systematic

```python
#%% workpiece dimensions
lx = 5.8  #longitude in x of the piece
ly = 3 #longitude in y of the piece

cte = 0.7 #constant surface height

PCDMIS_str = """PNT{:d}          =FEAT/POINT,CARTESIAN
            THEO/<{:.4f},{:.4f},{:.4f}>,<0,0,1>
            ACTL/<{:.4f},{:.4f},{:.4f}>,<0,0,1>
            MEAS/POINT,1
            HIT/BASIC,NORMAL,<{:.4f},{:.4f},{:.4f}>,<0,0,1>,<0.0077,1.4992,0.7311>,USE THEO=YES
            ENDMEAS/\n"""

PCDMIS_s = """{:.4f},'/t',{:.4f},'/t',{:.4f}>,<0,0,1>
            """
#%% Aligned Systematic Sampling

x = 40 #rows
z = 10 #columns
N_as = x * z

y = 1/x
r = 1/z

p = 1
while p > r:
    p = np.random.random(1)[0]
p <= r

q =1
while q > y:
    q = np.random.random(1)[0]

xy_as = np.zeros((N_as,2))

k = 0
for i in range(z):
    s = p + i * r
    for j in range(x):
        t = q + j * y

        xy_as[k] = [s,t]
        k += 1

xy_as[:,0] = lx * xy_as[:,0]
xy_as[:,1] = ly * xy_as[:,1]

plt.scatter(xy_as[:,0],xy_as[:,1])

f = open("PCDMIS_as.txt",'w')

for i in range(N_as):
    print(PCDMIS_str.format(i+2,xy_as[i,0],xy_as[i,1],cte,xy_as[i,0],xy_as[i,1],cte,xy_as[i,0],xy_as[i,1],cte))
    f.write(PCDMIS_str.format(i+2,xy_as[i,0],xy_as[i,1],cte,xy_as[i,0],xy_as[i,1],cte,xy_as[i,0],xy_as[i,1],cte))
f.close()

np.savetxt('Aligned_Systematic.txt',xy_as)
```

Halton-Zaremba

```python
import numpy as np
import matplotlib.pyplot as plt

#%% workpiece dimensions
lx = 5.8  #longitude in x of the piece
ly = 3 #longitude in y of the piece

cte = 0.7 #constant surface height

PCDMIS_str = """PNT{:d}         =FEAT/POINT,CARTESIAN
          THEO/<{:.4f},{:.4f},{:.4f}>,<0,0,1>
          ACTL/<{:.4f},{:.4f},{:.4f}>,<0,0,1>
          MEAS/POINT,1
          HIT/BASIC,NORMAL,<{:.4f},{:.4f},{:.4f}>,<0,0,1>,<0.0077,1.4992,0.7311>,USE THEO=YES
          ENDMEAS/\n"""

PCDMIS_s = """{:.4f},'/t',{:.4f},'/t',{:.4f}>,<0,0,1>
          """

#%% Halton-Zaremba Sampling

K_hz = 9
N_hz = 2**K_hz

pq = np.zeros((N_hz,2))
xy_hz = np.zeros((N_hz,2))

for i in range(N_hz):
    pq[i][0] = i/N_hz

    g = 0
    for j in range(K_hz):
        if j%2 == 0:
            g = g + (np.floor(i/(2**j))%2)*2**(-j-1)
        else:
            g = g + (1-np.floor(i/(2**j))%2)*2**(-j-1)

    pq[i][1] = g

xy_hz[:,0] = lx * pq[:,0]
xy_hz[:,1] = ly * pq[:,1]

plt.scatter(xy_hz[:,0],xy_hz[:,1])

f = open("PCDMIS_hz.txt",'w')

for i in range(N_hz):
    print(PCDMIS_str.format(i+2,xy_hz[i,0],xy_hz[i,1],cte,xy_hz[i,0],xy_hz[i,1],cte,xy_hz[i,0],xy_hz[i,1],cte))
    f.write(PCDMIS_str.format(i+2,xy_hz[i,0],xy_hz[i,1],cte,xy_hz[i,0],xy_hz[i,1],cte,xy_hz[i,0],xy_hz[i,1],cte))
f.close()

np.savetxt('Haton-Zaremba.txt',xy_hz)
```

Hammersley

```python
import numpy as np
import matplotlib.pyplot as plt

#%% workpiece dimensions
lx = 5.8  #longitude in x of the piece
ly = 3 #longitude in y of the piece

cte = 0.7 #constant surface height

PCDMIS_str = """PNT{:d}          =FEAT/POINT,CARTESIAN
            THEO/<{:.4f},{:.4f},{:.4f}>,<0,0,1>
            ACTL/<{:.4f},{:.4f},{:.4f}>,<0,0,1>
            MEAS/POINT,1
            HIT/BASIC,NORMAL,<{:.4f},{:.4f},{:.4f}>,<0,0,1>,<0.0077,1.4992,0.7311>,USE THEO=YES
            ENDMEAS/\n"""

PCDMIS_s = """{:.4f},'/t',{:.4f},'/t',{:.4f}>,<0,0,1>
            """

#%% Hammersley Sampling

N_h=400 #sample quantity


st = np.zeros((N_h,2))
xy_h = np.zeros((N_h,2))

K_h = int(np.ceil(np.log2(N_h)))

for i in range(N_h):
    st[i][0] = i/N_h

    t_aux = 0  # that will be added to the array position
    for j in range(K_h): #to K although the eq is K-1 because Python starts in 0
        t_aux = t_aux + (np.floor(i/(2**j))%2)*2**(-j-1)

    st[i][1] = t_aux

xy_h[:,0] = lx * st[:,0]
xy_h[:,1] = ly * st[:,1]

plt.scatter(xy_h[:,0],xy_h[:,1])

f = open("PCDMIS_h.txt",'w')

for i in range(N_h):
    print(PCDMIS_str.format(i+2,xy_h[i,0],xy_h[i,1],cte,xy_h[i,0],xy_h[i,1],cte,xy_h[i,0],xy_h[i,1],cte))
    f.write(PCDMIS_str.format(i+2,xy_h[i,0],xy_h[i,1],cte,xy_h[i,0],xy_h[i,1],cte,xy_h[i,0],xy_h[i,1],cte))
f.close()

np.savetxt('Hammersley.txt',xy_h)
```

APPENDIX B: Brown & Sharpe Microval PFx™ 454 and FaroArm® Scan Platinum Specifications

CMM	Brown & Sharpe MicroVal PFx™ 454
 Figure 37 Brown & Sharpe MicroVal PFx™ 454	
Linear Accuracy	0.0002 in
Resolution	0.00004 in
Measurement repeatability	0.00015 in
Measure Range	14″ x 16″ x 12″
Work Capacity	18″ x 24″ x 15″

AACMM	Faro Arm® Platinum
Figure 38 FaroArm® Platinum with ScamArm®	
Precision	up to 0.020mm
Number of Axis	7
Degrees of Freedom	6
Ball probe	3mm = 0.11811in
Laser ScanArm® accuracy ("Faro Laser ScanArm® V3 (PDF)," 2010)	accuracy of up to 0.035mm (0.0014in)
Points per line ("FaroArm® Platinum (PDF)," 2010)	640 points/lineScan. Rate:30frames/second30fpsx 640points/line = 19,200 points/sec

APPENDIX C Rough pass values

SAMPLE 1 Steel 1012 – Rough pass					
Aligned Systematic Sampling					
Number of Points	**Average Measured Position Z**	**Average Gap Vector X**	**Average Gap Vector Y**	**Average Gap Vector Z**	**Average Gap Distance**
400	0.73185725	-0.0000075	-0.00015175	0.00187675	0.001873
Hammersley					
Number of Points	**Average Measured Pos. Z**	**Average Gap Vec. X**	**Average Gap Vec. Y**	**Average Gap Vec. Z**	**Average Gap Dist.**
400	0.732233	-9.1E-05	0.000028	0.002232	0.002239
Halton-Zaremba					
Number of Points	**Average Measured Pos. Z**	**Average Gap Vec. X**	**Average Gap Vec. Y**	**Average Gap Vec. Z**	**Average Gap Dist.**
512	0.731603516	-2.53906E-05	4.55078E-05	0.001683008	0.001732227

SAMPLE 2 Steel 1012 – Rough pass					
Aligned Systematic Sampling					
Number of Points	**Average Measured Position Z**	**Average Gap Vector X**	**Average Gap Vector Y**	**Average Gap Vector Z**	**Average Gap Distance**
400	0.736745	-2.5E-07	-0.0000125	0.0027575	0.00276175
Hammersley					
Number of Points	**Average Measured Pos. Z**	**Average Gap Vec. X**	**Average Gap Vec. Y**	**Average Gap Vec. Z**	**Average Gap Dist.**
400	0.7365535	-0.000033	0.00023225	0.00260575	0.00286225
Halton-Zaremba					
Number of Points	**Average Measured Pos. Z**	**Average Gap Vec. X**	**Average Gap Vec. Y**	**Average Gap Vec. Z**	**Average Gap Dist.**
512	0.73657832	-3.55469E-05	0.000295508	0.002642969	0.00279941

SAMPLE 3 Steel 1012 – Rough pass					
Aligned Systematic Sampling					
Number of Points	Average Measured Position Z	Average Gap Vector X	Average Gap Vector Y	Average Gap Vector Z	Average Gap Distance
400	0.73069375	-0.0000025	-0.000397	0.00143575	0.00131925
Hammersley					
Number of Points	Average Measured Pos. Z	Average Gap Vec. X	Average Gap Vec. Y	Average Gap Vec. Z	Average Gap Dist.
400	1.493642356	0.730270175	5.51378E-06	-9.02256E-05	0.001138095
Halton-Zaremba					
Number of Points	Average Measured Pos. Z	Average Gap Vec. X	Average Gap Vec. Y	Average Gap Vec. Z	Average Gap Dist.
512	0.730514481	-4.50098E-06	-1.99609E-05	0.001394716	0.001452642

SAMPLE 4 Aluminum 6061 – Rough pass					
Aligned Systematic Sampling					
Number of Points	Average Measured Position Z	Average Gap Vector X	Average Gap Vector Y	Average Gap Vector Z	Average Gap Distance
400	0.73332275	0.000134	-0.00074675	0.0014515	0.00188875
Hammersley					
Number of Points	Average Measured Pos. Z	Average Gap Vec. X	Average Gap Vec. Y	Average Gap Vec. Z	Average Gap Dist.
400	0.7335065	-0.0005565	-0.000244	0.001866	0.00265525
Halton-Zaremba					
Number of Points	Average Measured Pos. Z	Average Gap Vec. X	Average Gap Vec. Y	Average Gap Vec. Z	Average Gap Dist.
512	0.733790625	-0.000327344	0.000100195	0.002063672	0.00254688

SAMPLE 5 Aluminum 6061 – Rough pass					
Aligned Systematic Sampling					
Number of Points	**Average Measured Position Z**	**Average Gap Vector X**	**Average Gap Vector Y**	**Average Gap Vector Z**	**Average Gap Distance**
400	0.73589375	0.0000855	-0.00112675	0.000648	0.00073375
Hammersley					
Number of Points	**Average Measured Pos. Z**	**Average Gap Vec. X**	**Average Gap Vec. Y**	**Average Gap Vec. Z**	**Average Gap Dist.**
400	0.73574625	-0.00007525	-0.00073625	0.0006105	0.0004575
Halton-Zaremba					
Number of Points	**Average Measured Pos. Z**	**Average Gap Vec. X**	**Average Gap Vec. Y**	**Average Gap Vec. Z**	**Average Gap Dist.**
512	0.735574805	-2.69531E-05	-0.000457422	0.000461328	0.00051328

SAMPLE 6 Aluminum 6061 – Rough pass					
Aligned Systematic Sampling					
Number of Points	**Average Measured Position Z**	**Average Gap Vector X**	**Average Gap Vector Y**	**Average Gap Vector Z**	**Average Gap Distance**
400	0.7322705	0.00004	-0.00050825	0.001385	0.001133
Hammersley					
Number of Points	**Average Measured Pos. Z**	**Average Gap Vec. X**	**Average Gap Vec. Y**	**Average Gap Vec. Z**	**Average Gap Dist.**
400	0.7322325	-0.00024825	0.000111	0.001477	0.001352
Halton-Zaremba					
Number of Points	**Average Measured Pos. Z**	**Average Gap Vec. X**	**Average Gap Vec. Y**	**Average Gap Vec. Z**	**Average Gap Dist.**
512	0.732387891	-0.000214063	0.000246875	0.001542773	0.00172578

APPENDIX D Finish pass values

SAMPLE 1 Steel 1012 – Finish pass					
Aligned Systematic Sampling					
Number of Points	Average Measured Position Z	Average Gap Vector X	Average Gap Vector Y	Average Gap Vector Z	Average Gap Distance
400	0.673286	-4E-05	-5E-05	0.00192525	0.00201375
Hammersley					
Number of Points	Average Measured Pos. Z	Average Gap Vec. X	Average Gap Vec. Y	Average Gap Vec. Z	Average Gap Dist.
400	0.673324	5.51E-06	-2.3E-05	0.001911	0.001938
Halton-Zaremba					
Number of Points	Average Measured Pos. Z	Average Gap Vec. X	Average Gap Vec. Y	Average Gap Vec. Z	Average Gap Dist.
512	0.673103	-1.9E-05	4.73E-05	0.001673	0.001833

SAMPLE 2 Steel 1012 – Finish pass					
Aligned Systematic Sampling					
Number of Points	Average Measured Position Z	Average Gap Vector X	Average Gap Vector Y	Average Gap Vector Z	Average Gap Distance
400	0.683699	-3.4E-05	-0.00038	0.001024	0.001206
Hammersley					
Number of Points	Average Measured Pos. Z	Average Gap Vec. X	Average Gap Vec. Y	Average Gap Vec. Z	Average Gap Dist.
400	0.683523	-9E-05	-0.00014	0.000922	0.000993
Halton-Zaremba					
Number of Points	Average Measured Pos. Z	Average Gap Vec. X	Average Gap Vec. Y	Average Gap Vec. Z	Average Gap Dist.
512	0.683409	-5.5E-05	-7.4E-05	0.000748	0.000858

SAMPLE 3 Steel 1012 – Finish pass					
Aligned Systematic Sampling					
Number of Points	**Average Measured Position Z**	**Average Gap Vector X**	**Average Gap Vector Y**	**Average Gap Vector Z**	**Average Gap Distance**
400	0.67645	-7.6E-05	-0.00071	-0.0004	-0.0002
Hammersley					
Number of Points	**Average Measured Pos. Z**	**Average Gap Vec. X**	**Average Gap Vec. Y**	**Average Gap Vec. Z**	**Average Gap Dist.**
400	0.676033	-1.1E-05	-0.00022	-0.00118	-0.00141
Halton-Zaremba					
Number of Points	**Average Measured Pos. Z**	**Average Gap Vec. X**	**Average Gap Vec. Y**	**Average Gap Vec. Z**	**Average Gap Dist.**
512	0.676222	-3.4E-05	-0.00027	-0.0009	-0.00085

SAMPLE 4 Aluminum 6061 – Finish pass					
Aligned Systematic Sampling					
Number of Points	**Average Measured Position Z**	**Average Gap Vector X**	**Average Gap Vector Y**	**Average Gap Vector Z**	**Average Gap Distance**
400	0.671566	-2.8E-05	-0.00051	0.000174	0.000559
Hammersley					
Number of Points	**Average Measured Pos. Z**	**Average Gap Vec. X**	**Average Gap Vec. Y**	**Average Gap Vec. Z**	**Average Gap Dist.**
400	0.671749	1.75E-06	-0.00016	0.000116	0.000266
Halton-Zaremba					
Number of Points	**Average Measured Pos. Z**	**Average Gap Vec. X**	**Average Gap Vec. Y**	**Average Gap Vec. Z**	**Average Gap Dist.**
512	0.671793	-2.9E-05	-0.00013	0.000129	0.000198

SAMPLE 5 Aluminum 6061 – Finish pass					
Aligned Systematic Sampling					
Number of Points	**Average Measured Position Z**	**Average Gap Vector X**	**Average Gap Vector Y**	**Average Gap Vector Z**	**Average Gap Distance**
400	0.671731	2.35E-05	-8.5E-05	0.002276	0.002291
Hammersley					
Number of Points	**Average Measured Pos. Z**	**Average Gap Vec. X**	**Average Gap Vec. Y**	**Average Gap Vec. Z**	**Average Gap Dist.**
400	0.671819	-6.5E-05	-9E-05	0.002381	0.002331
Halton-Zaremba					
Number of Points	**Average Measured Pos. Z**	**Average Gap Vec. X**	**Average Gap Vec. Y**	**Average Gap Vec. Z**	**Average Gap Dist.**
512	0.671813	-1.5E-05	3.4E-05	0.002436	0.002522

SAMPLE 6 Aluminum 6061 – Finish pass					
Aligned Systematic Sampling					
Number of Points	**Average Measured Position Z**	**Average Gap Vector X**	**Average Gap Vector Y**	**Average Gap Vector Z**	**Average Gap Distance**
400	0.669126	-2.2E-05	-0.00057	-0.00696	-0.00707
Hammersley					
Number of Points	**Average Measured Pos. Z**	**Average Gap Vec. X**	**Average Gap Vec. Y**	**Average Gap Vec. Z**	**Average Gap Dist.**
400	0.669248	-6.9E-05	-0.00024	-0.00645	-0.00652
Halton-Zaremba					
Number of Points	**Average Measured Pos. Z**	**Average Gap Vec. X**	**Average Gap Vec. Y**	**Average Gap Vec. Z**	**Average Gap Dist.**
512	0.668688	-8.2E-06	-0.00013	-0.00694	-0.00699

APPENDIX E Macro code to clean CMM Sampling data using Microsoft® Excel

```vba
Sub deleteSelectedRow()

    'Source: http://powerspreadsheets.com/

    'For further information: http://powerspreadsheets.com/excel-vba-delete-row/



    Selection.EntireRow.Delete


End Sub
```

(Gomez, n.d.)